J Physiol 602.17 (2024) pp 4195–4213

The Journal of Physiology

Multiple layers of diversity govern the cell type specificity of GABAergic input received by mouse subicular pyramidal neurons

Nancy Castro Borjas[1], Max Anstötz[2] and Gianmaria Maccaferri[1]

[1]*Department of Neuroscience, Feinberg School of Medicine, Northwestern University, Chicago, USA*
[2]*Institute of Anatomy II, Medical Faculty, Heinrich-Heine-University, Düsseldorf, Germany*

Handling Editors: Katalin Toth & Samuel Young

The peer review history is available in the Supporting Information section of this article (https://doi.org/10.1113/JP286679#support-information-section).

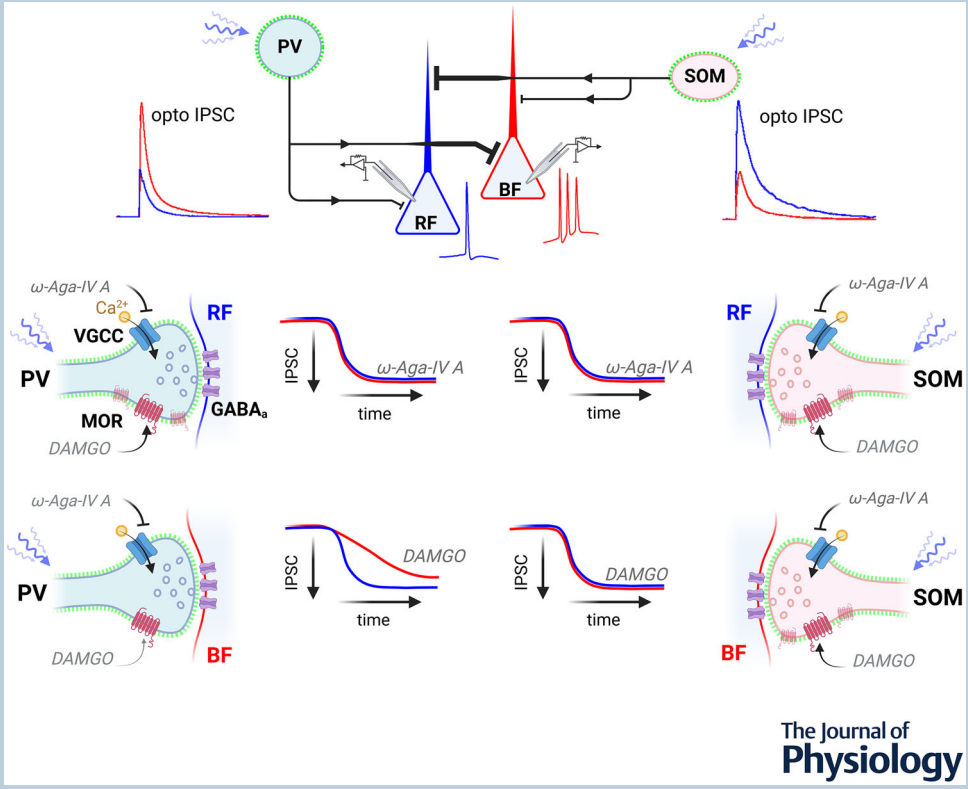

Abstract The subiculum is a key region of the brain involved in the initiation of pathological activity in temporal lobe epilepsy, and local GABAergic inhibition is essential to prevent

Nancy Castro Borjas received her bachelor's degree in biochemistry and biotechnology from Minnesota State University Moorhead in 2017. She is currently enrolled as a graduate student in the Northwestern University Interdepartmental Neuroscience programme. Nancy's current research interests are focused on elucidating the functional architecture of cortical circuits in physiological and pathological conditions. Nancy's goal is to continue to expand her knowledge of advanced morpho-functional techniques with the hope of investigating cellular and molecular mechanisms that can be the target of future therapies for brain disorders.

DOI: 10.1113/JP286679

subicular-originated epileptiform discharges. Subicular pyramidal cells may be easily distinguished into two classes based on their different firing patterns. Here, we have compared the strength of the GABAa receptor-mediated inhibitory postsynaptic currents received by regular- *vs*. burst-firing subicular neurons and their dynamic modulation by the activation of μ opioid receptors. We have taken advantage of the sequential re-patching of the same cell to initially classify pyramidal neurons according to their firing patters, and then to measure GABAergic events triggered by the optogenetic stimulation of parvalbumin- and somatostatin-expressing interneurons. Activation of parvalbumin-expressing cells generated larger responses in postsynaptic burst-firing neurons whereas the opposite was observed for currents evoked by the stimulation of somatostatin-expressing interneurons. In all cases, events depended critically on ω-agatoxin IVA- but not on ω-conotoxin GVIA-sensitive calcium channels. Optogenetic GABAergic input originating from both parvalbumin- and somatostatin-expressing cells was reduced in amplitude following the exposure to a μ opioid receptor agonist. The kinetics of this pharmacological sensitivity was different in regular- *vs*. burst-firing neurons, but only when responses were evoked by the activation of parvalbumin-expressing neurons, whereas no differences were observed when somatostatin-expressing cells were stimulated. In conclusion, our results show that a high degree of complexity regulates the organizing principles of subicular GABAergic inhibition, with the interaction of pre- and postsynaptic diversity at multiple levels.

(Received 2 April 2024; accepted after revision 23 July 2024; first published online 14 August 2024)
Corresponding author G. Maccaferri: Department of Neuroscience, Northwestern University, Feinberg School of Medicine, 310 E Chicago Ave., Tarry Blg Rm 5–707 M211, Chicago, IL 60611, USA. Email: g-maccaferri@northwestern.edu

Abstract figure legend We have studied the pre- and postsynaptic factors involved in the regulation of synaptic inhibition in distinct subicular microcircuits. Parvalbumin- (PV) and somatostatin-expressing (SOM) interneurons produce optogenetically evoked IPSCS (opto IPSC) mediated by GABAa receptors (GABAa) with an opposite amplitude bias for regular-firing (RF) *vs*. burst-firing (BF) pyramidal cells. In all cases, IPSCs require the functional integrity of P/Q voltage-gated calcium channels (VGCCs) sensitive to ω-agatoxin IVA (ω-aga-IVA), indicating similar mechanisms of release. In contrast, the kinetics of IPSC suppression by the presynaptic μ opioid receptor (MOR) triggered by the agonist [D-Ala2, *N*-MePhe4, Gly-ol]-enkephalin (DAMGO) was slower in BF compared to RF cells. We propose, as a potential explanation, a lower density of these receptors at the presynaptic terminals of PV-interneurons contacting BF cells. In summary, these results highlight the existence of multiple complex layers of diversity governing the cell type specificity of GABAergic input received by subicular pyramidal cells.

Key points

- Optogenetic stimulation of parvalbumin- and somatostatin-expressing interneurons (PVs and SOMs) triggers inhibitory postsynaptic currents (IPSCs) in both regular- and burst-firing (RFs and BFs) subicular pyramidal cells.
- The amplitude of optogenetically evoked IPSCs from PVs (PV-opto IPSCs) is larger in BFs whereas IPSCs generated by the light activation of SOMs (SOM-opto IPSCs) are larger in RFs.
- Both PV- and SOM-opto IPSCs critically depend on ω-agatoxin IVA-sensitive P/Q type voltage-gated calcium channels, whereas no major effects are observed following exposure to ω-conotoxin GVIA, suggesting no significant involvement of N-type channels.
- The amplitude of both PV- and SOM-opto IPSCs is reduced by the probable pharmacological activation of presynaptic μ opioid receptors, with a faster kinetics of the effect observed in PV-opto IPSCs from RFs *vs*. BFs, but not in SOM-opto IPSCs.
- These results help us understand the complex interactions between different layers of diversity regulating GABAergic input onto subicular microcircuits.

Introduction

The subiculum is a critical output of the hippocampal formation that targets several cortical and subcortical regions (Böhm et al., 2018). This widespread anatomical connectivity explains its involvement in various and diverse functions, which include the processing of spatial information, movement, memory and the response to stress (O'Mara et al., 2009). Subicular circuits are also believed to play important roles in the initiation and propagation of pathological activity in temporal lobe epilepsy (TLE, Lévesque & Avoli, 2020). A variety of abnormal discharge patterns (interictal and preictal bursts, as well as electrographic seizures) has been observed in the subiculum of human patients with TLE and in epileptic animals *in vivo* and *in vitro* (Cohen et al., 2002; Huberfeld et al., 2011; Wang et al., 2017).

Studies on the cellular microarchitecture of the subiculum have revealed the presence of functionally distinct excitatory principal neurons (pyramidal cells, PCs), classically divided by their firing patterns into regular- or burst-firing cells (RFs and BFs, respectively, Behr et al., 1996; Böhm et al., 2015; Cembrowski et al., 2018; Fiske et al., 2020; Greene & Totterdell, 1997; Jarsky et al., 2008; Kim & Spruston, 2012; Mattia et al., 1993; Menendez de la Prida, 2003; Menendez de la Prida et al., 2003; Pannuccio et al., 2012; Staff et al., 2000; Taube, 1993). At the local network level, subicular PCs possess a high degree of excitatory interconnectivity (overall ∼5%, Böhm et al, 2015; Fiske et al. 2020), compared what has been reported for principal neurons in other regions of the hippocampal formation (∼1% in the CA3, Guzman et al., 2016 and CA1 subfields, Deuchars & Thomson, 1996). These local excitatory synapses occur predominantly onto basal dendrites (Fiske et al. 2020), which are relatively close to the axon, where the action potential is usually generated (Colbert & Johnston, 1996). The power of these intrinsic excitatory connections is highlighted by the observation that the disruption of local GABAergic inhibition in subicular slices, surgically isolated from their adjacent regions, is sufficient to initiate spontaneous epileptiform discharges (Fiske et al., 2020; Anstötz et al., 2021). Both this physiological hyperconnectivity and the vulnerability to pathologically reduced inhibition are consistent with a prominent theory of human TLE (Miles et al., 2012) highlighting the key role of the subiculum as an epileptic focus initiating abnormal activity. In particular, the subicular-specific downregulation of the KCC2 transporter (a critical regulator of GABAa receptor-mediated transmission, Palma et al., 2006; de Guzman et al., 2006; Huberfeld et al., 2007) observed in TLE would lead to altered inhibition and trigger the initiation of epileptiform synchronization.

The anti-epileptic role of physiological GABAergic inhibition depends on synaptic release of GABA from populations of interneurons (INTs, Pelkey et al., 2017) that are endowed with a high degree of morpho-functional heterogeneity (Maccaferri & Lacaille, 2003).

Despite many studies addressing the issue of diversity of interneurons in the hippocampus proper (reviewed by Somogyi & Klausberger, 2005), less is known about the cell type specific organization of GABAergic networks in the subiculum (Benini & Avoli, 2005; Böhm et al., 2015; Menendez de la Prida, 2003; Menendez de la Prida et al, 2003; Pannuccio et al., 2012).

We aimed to gain novel insights into the functional architecture of subicular GABAergic networks by studying the interaction between the diversity within INTs and PCs at multiple levels. First, we contrasted the static properties and dependence on specific voltage-gated calcium channels of GABAergic inhibitory postsynaptic currents (IPSCs) originating from INTs targeting perisomatic *vs*. dendritic postsynaptic domains (Miles et al., 1996) of functionally distinct PCs (RFs and BFs). Then, we investigated the dynamic sensitivity of these specific IPSCs to the activation of μ opioid receptors (MORs), which modulate GABA release in several regions of the brain (Reeves et al., 2022). This is important for several reasons. First, the relative degree of GABAergic inhibition between perisomatic and dendritic postsynaptic domains may affect the local spike threshold (Colbert & Johnston, 1996; Gasparini et al., 2004; Golding & Spruston, 1998), which is critical for determining the location of the action potential initiation site. This would be predicted to bear consequences on cell firing and synaptic plasticity, thus affecting the network computational properties. Second, a differential response to MOR activation in IPSCs onto RFs *vs*. BFs may suggest mechanistic pharmacological regulations affecting the different behaviours mediated by these PC subtypes (Cembrowski et al., 2018).

Our results indicate that multiple layers of diversity govern the cell type specificity of GABAergic input and its regulation by MORs on subicular PCs, thus increasing the complexity of how fast synaptic inhibition acts physiologically in generating network computations and in preventing epileptiform activity.

Materials and methods

Ethical approval

All animal procedures used in this study were approved by the Institutional Animal Care and Use Committee of Northwestern University (animal protocols #IS0000552 and IS00026872) in accordance with the animal guidelines provided by the National Institute of Health and by *The Journal of Physiology*.

Animals

The following mouse strains were obtained from The Jackson Laboratory (Bar Harbor, ME, USA): PV-Cre (RRID:IMSR_JAX:008069), SOM-Cre (RRID:IMSR_JAX:028864) and ChR2 (H134R)-eYFP (RRID:IMSR_JAX:012569). These lines were maintained as homozygous and crossed to generate animals conditionally expressing ChR2 (H134R)-EYP [PV-ChR2 (H134R)-eYFP and SOM-ChR2 (H134R)-eYFP)]. Experiments were conducted in male and female mice between postnatal ages of P24–P44. Mice were housed on a 14/10 h light/dark cycle and given *ad libitum* access to food and water. The number of animals used for each experiment is indicated in the Results.

Acute slice preparation

Mice were deeply anaesthetized (open drop, 0.5 mL of isoflurane per 500 mL volume of anaesthesia jar). The induction chamber had a separate platform to prevent direct contact between the animal and the anaesthetic. Following clinical indications of deep anaesthesia (reduction of respiratory rate, lack of righting reflex and responses to noxious stimuli) decapitation was performed. The brain was carefully removed and glued to a specimen block in a chamber filled with cooled ACSF with the following composition (in mM): 130 NaCl, 24 $NaHCO_3$, 3.5 KCl, 1.25 NaH_2PO_4, 1 $CaCl_2$, 2 $MgSO_4$ and 10 glucose, saturated with 95% O_2, 5% CO_2 at pH 7.4. Transverse sections (350 µm) of an entire brain hemisphere containing the hippocampal formation were cut using a vibratome (Leica VT 1200 S, Leica Biosystems, Wetzlar, Germany). Slices were recovered at 30°C for about 30 min and then kept at room temperature until use.

Electrophysiological recordings and analysis

Slices were transferred to a recording chamber positioned under a direct microscope (Scientifica, Brambleside, UK) equipped with oblique illumination optics (Olympus) and an infrared camera system (Zyla, Andor, Belfast, Northern Ireland). Cells were visualized with a 60× infrared water-immersion objective (Olympus, Tokyo, Japan). Slices were superfused with preheated ACSF (29–31°C, TC-324B, Warner Instruments, Hamden, CT, USA) with the following composition (in mM): 130 NaCl, 24 $NaHCO_3$, 3.5 KCl, 1.25 NaH_2PO_4, 2 $CaCl_2$,1 $MgCl_2$, 10 glucose, saturated with 95% O_2, 5% CO_2 at pH 7.4.

Pipettes were pulled from thin borosilicate capillaries (G150TF-4, Warner Instruments) with a resistance of ∼2 MΩ when filled with an internal solution containing (for current-clamp recordings) the following (in mM): 125 CH_3KO_4S, 10 NaCl, 16 $KHCO_3$, 4 ATP-Mg, 0.3 GTP-Na and 0.25% biocytin equilibrated with 95% O_2, 5% CO_2 at pH 7.3. Voltage clamp recordings were performed with an internal solution containing (in mM): 125 CH_3CsO_3S, 16 $KHCO_3$,4 ATP-Mg_2, 0.3 GTP-Na_2, 10 QX-314-Cl, 1 EGTA and 0.25% biocytin equilibrated with 95% O_2, 5% CO_2 at pH 7.3. Data were acquired with a Multiclamp 700A amplifier (Molecular Devices, Sunnyvale, CA, USA). Series resistances were monitored throughout experiments and measured, but not corrected. Signals were filtered at 3 kHz and digitized at a minimum of 20 kHz using a Digidata 1550A digitizer and the Clampex11 program (Molecular Devices). Recorded waveforms were analysed using the following programs: pClamp (Molecular Devices, RRID:SCR_011323), OriginPro2020 (Origin Lab Corporation, Northampton, MA, USA, RRID:SCR_014212) and Prism (GraphPad Software LLC, La Jolla, CA, USA, RRID:SCR_002798).

Firing pattern protocol

From a holding membrane voltage of ∼−65 mV, cells were injected with a 1 s current pulse of increasing amplitude in 50 pA steps every 5 s. The first suprathreshold responses were used for the measurement of the interspike frequency between the first two action potentials and for cell type classification.

Opto IPSC recordings

Neurons were maintained at a holding potential of +10 mV to increase the driving force for GABAa receptor-mediated events and to avoid potential contamination from spontaneous excitatory currents. Liquid junction potential was estimated (+12.4 mV) according to the stationary Nernst–Planck equation (Marino et al., 2014) using LJPcalc (RRID:SCR_025044). Because it introduced the same systematic error in all opto IPSC recordings, it was not corrected in the presentation of the results.

Optogenetic stimulation

Control of specific cellular populations expressing ChR2[H134R]-eYFP was achieved by flashes of blue light of 0.5 ms duration generated by a collimated LED (460 nm, Prizmatix, Holon, Israel) attached to the epifluorescence port of the direct microscope. Light flashes were directed to the microscopic field via a mirror coupled to a 60× objective (1.0 NA).

Anatomical recovery of biocytin-filled cells

Slices with filled neurons were fixed for 24 h in 4% paraformaldehyde solution in 0.1 M PB at 4°C. The

material was then incubated free-floating for 20 min at room temperature in a solution containing 1% Triton X-100 and Alexa Fluor 594 streptavidin in PBS. Slices were then washed three times for 15 min with PBS, with the second washing step containing DAPI (1:10,000, Life Technologies, Carlsbad, CA, USA) and, lastly, mounted and coverslipped using Mowiol mounting medium.

Confocal microscopy

Images were acquired with a Leica SP8 STED confocal microscope, utilizing a 20×/0.75 NA oil (entire cell) lens and a 100×/1.4 NA oil (putative contact sites). Following acquisition, the image stacks were processed with the Leica Lightning deconvolution module. A maximum intensity projection of deconvoluted image stacks was then generated. For images of putative contact sites, the optical section was 1 µm.

Statistical analysis

Data comparison was performed using non-parametric tests. For non-paired samples from two groups, we compared the normalized average values of the amplitude of optogenetic responses measured at the last 2 min of the experiments ($n = 12$ sweeps) with the Mann–Whitney test (MW), whereas, in the case of more than two groups, we used the Kruskal–Wallis with Dunn's *post hoc* test (KWD). Differences between cumulative distributions were evaluated using the Kolmogorov–Smirnoff test (KS). For before–after paired samples, we compared the average values of the absolute amplitude of optogenetic responses (or series resistance) immediately before and after the addition of the drug at the end of the experiment. Values were calculated from data collected during 1 or 2 min ($n = 6$ sweeps, gabazine experiment and $n = 12$ sweeps, (RS)-α-Methyl-4-carboxyphenylglycine (MCGP) experiment, respectively) and compared using the Wilcoxon test (W). The significance of a slope in linear regression analysis was determined by an F test (F). Lastly, we used two-way repeated measurements ANOVA on ranks (TWAR) to compare the kinetics of the time course of opto IPSCs following the pharmacological activation of MOR under various experimental conditions. The level of significance for all tests was $P < 0.05$.

Drugs

Gabazine was prepared as a 25 mM stock solution in water and used in experiments at 12.5 µM. ω-Agatoxin IVA and ω-conotoxin GVIA were purchased from Alomone Labs (Jerusalem, Israel). Both ω-agatoxin IVA and ω-conotoxin GVIA were dissolved in milliQ water and used in experiments at 600 nM and 1 µM with added 2% BSA, respectively. [D-Ala2, *N*-MePhe4, Gly-ol]-enkephalin (DAMGO) was purchased from Abcam (Cambridge, MA, USA) and prepared as a 5 mM stock solution in milliQ water to be used in experiments as 5 µM with 2% BSA. Naloxone was prepared as a 10 mM stock solution and used as 10 µM. MCGP was purchased from Tocris (Minneapolis, MN, USA), prepared as a 100 mM stock solution and used at 500 µM.

Results

To study the cellular specificity of GABAergic inhibition in subicular circuits, we used *ex vivo* slices prepared from PV-ChR2(H134R)-eYFP and SOM-ChR2(H134R)-eYFP mice, which allow the optogenetic activation of parvalbumin- and somatostatin-expressing interneurons (PVs and SOMs), respectively. Short light stimulation (0.5 ms flash duration) generated outward IPSCs in voltage-clamped PCs held at +10 mV (Fig. 1*A*, *B* and *C*). These events were fully blocked by the GABAa receptor-specific antagonist gabazine (12.5 µM). The peak amplitude of optogenetically evoked IPSCs from PVs (PV-opto IPSCs) was 2.8 nA (mean), 1.1 nA (SD) in control compared to 0.0 nA, 0.0 nA (SD) in the presence of the drug ($n = 10$ cells, 2 mice, $P = 0.002$, W). Similarly, gabazine blocked light-evoked IPSCs generated by the stimulation of SOMs (SOM-opto IPSCs, from 2.4 nA (mean), 1.0 nA (SD) in control to 0.0 nA (mean), 0.0 nA (SD) following the addition of gabazine, $n = 10$ cells, 2 mice, $P = 0.002$, W). No differences were found either in the effect of gabazine on opto IPSCs evoked by PV *vs*. SOM stimulation ($P = 0.912$, MW) or in the series resistance drift during PV- *vs*. SOM-opto IPSC recordings (MW, $P = 0.631$).

Although these results show the reliable generation of GABAa receptor-mediated opto IPSCs originating from PVs and SOMs, the specific organization of these inputs onto functionally distinct PCs would also require their firing pattern characterization. However, the pipette solution used for voltage-clamp recordings, which included Cs^+ as the main cation and QX314 to block intrinsic conductances, prevented this type of evaluation. In contrast, when electrodes were filled with a 'current-clamp intracellular solution' (K^+ as the main cation and without blockers of intrinsic conductances, Fig. 1*D*), the injection of near-threshold currents produced trains of spikes revealing the typical phenotype of RFs and BFs, which were easily distinguished by the frequency of the first action potentials in the train. These values were distributed bimodally, with a clear separation between the two peaks ($n = 247$ recorded cells, $n = 67$ mice, Fig. 1*E*). The proportion of RFs *vs*. BFs was roughly equal (RFs, 48% and BFs, 52%), similar to what was previously reported (Fiske et al., 2020). When initial

frequencies were plotted against the developmental age of the animals used, no significant slope was observed ($P = 0.879$ for RF, $n = 118$ cells and $P = 0.505$ for BF PCs, $n = 129$ cells, F, Fig. 1*E*). Direct comparison of the frequencies measured in female *vs.* male mice also failed to reveal significant differences ($P = 0.414$ for RF PCs, $n = 60$ and $n = 58$ cells from male and female mice, respectively, MW and $P = 0.870$ for BF PCs, $n = 67$ and $n = 62$ cells from male and female animals, respectively, MW, Fig. 1*F*).

In conclusion, under our experimental conditions, neither age nor sex appeared to shape the firing pattern response of subicular PCs, which validated the use of this simple parameter for their classification.

To achieve a quantitative measurement of the opto IPSCs from functionally distinguished RFs and BFs, we took advantage of a two-step recording approach (Fig. 2*A*,*B*). First, the firing pattern of the cell under study was collected with a 'current-clamp intracellular solution' in the electrode, thus allowing the classification

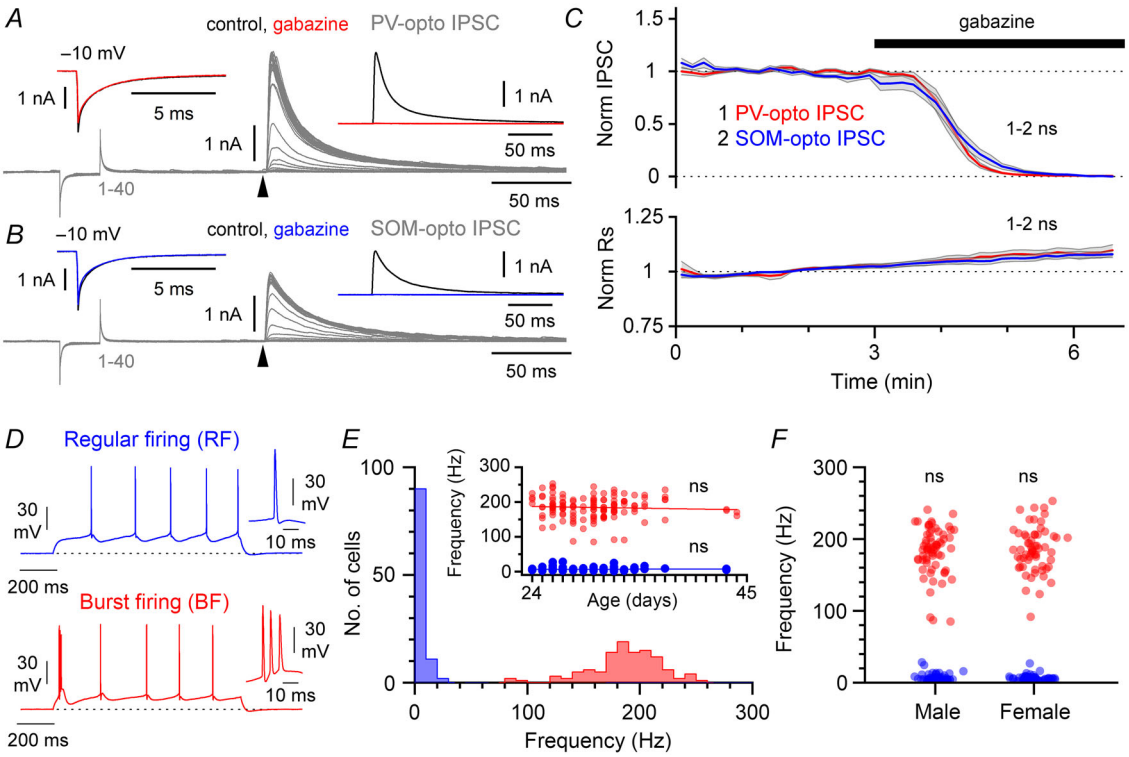

Figure 1. Voltage- and current-clamp experiments showing GABAa receptor-mediated opto IPSCs and firing patterns recorded from subicular pyramidal cells (PCs).
A, representative experiment showing the time-dependent block by the GABAa antagonist gabazine (12.5 μM) of responses evoked by the repetitive (40 events, triggered 0.1 Hz, 1–40, grey traces) optogenetic stimulation of parvalbumin-expressing interneurons (PV-opto IPSC). PC held in voltage-clamp at +10 mV. Optogenetic stimulation was preceded by a short voltage-clamp step (−10 mV) to assess the stability of the series resistances. Average traces of the first (control, black) and of the last minute (gabazine, red) of the experiment highlight the downward capacitive transient (left inset) and the IPSC (right inset, light flash is not indicated for clarity). *B*, identical to *A*, but for measurements performed on events evoked by the optogenetic of somatostatin-expressing interneurons (SOM-opto IPSC). *C*, summary plots (top) showing the time course of the normalized PV- and SOM-opto IPSCs (norm IPSC) during gabazine application (black bar) and (bottom) the stability of the normalized series resistance during the recordings (norm Rs). The effect of gabazine on PV- *vs.* SOM-IPSCs was not significantly different. The two experiments showed no differences in the series resistance changes. *D*, current-clamp recordings revealing the functional dichotomy of PCs. Note the representative traces of regular-firing (blue, RF) and burst-firing (red, BF) pyramidal neurons. First suprathreshold responses following the injection of current pulses (1 s duration) in 50 pA increments every 5 s. Threshold currents of the examples were 200 pA for the regular- and 150 pA for the burst-firing neuron. Insets show the first action potential(s) at an enhanced temporal scale. *E*, population analysis of the instantaneous firing frequency of the first spike pair for $n = 214$ PCs. Note the bimodal distribution and clear separation of the regular- and burst-firing cells. The inset shows the lack of correlation between the calculated frequency and the age of the animals used for the experiment. *F*, plot of individual values grouped according to the sex of the animals. Note the lack of differences in firing frequencies between the male and female groups. ns, $P > 0.05$. Data of the time course plot are shown as mean ± SEM. [Colour figure can be viewed at wileyonlinelibrary.com]

of the recorded neuron as either RF or BF. Then, the pipette was gently withdrawn, allowing the membrane to reseal. Lastly, the same neuron was re-patched with a 'voltage-clamp intracellular solution' for measurement of the opto IPSC originated from PVs and SOMs. Alternative approaches, such as filling the tip and remaining part of the pipette with current-clamp and voltage-clamp solutions, respectively, were ineffective because of the rapid mixing between the two compartments, which disrupted action potential waveforms (data not shown).

Similar to previously described in other parts of the hippocampal formation (Pelkey et al., 2017; Somogyi & Klausberger, 2005), PVs and SOMs target different postsynaptic domains (perisomatic and dendritic, respectively, Fig. 2*C*–*H*). As expected, PV-opto IPSCs had 20–80% shorter risetimes when compared to SOM-opto IPSCs [1.2 ms (mean), 0.6 ms (SD) *vs.* 2.3 ms (mean), 1.1 ms (SD), $n = 159$ and $n = 83$ PV- and SOM-opto IPSCs, from $n = 42$ and $n = 23$ mice, respectively, $P < 0.0001$ KS], which reflect the different location of the events (Fig. 2*I*, *J*)

Comparison of the size of opto IPSCs evoked from the selective activation of PVs and SOMs in functionally distinguished PCs revealed two layers of diversity. As shown in Fig. 3, the amplitude of the evoked events depended both on the type of presynaptic INT stimulated and on the functional subtype of postsynaptic PC examined. PV-opto IPSCs were of larger amplitudes in BFs compared to RFs (Fig. 3*A*, *B*), whereas the opposite

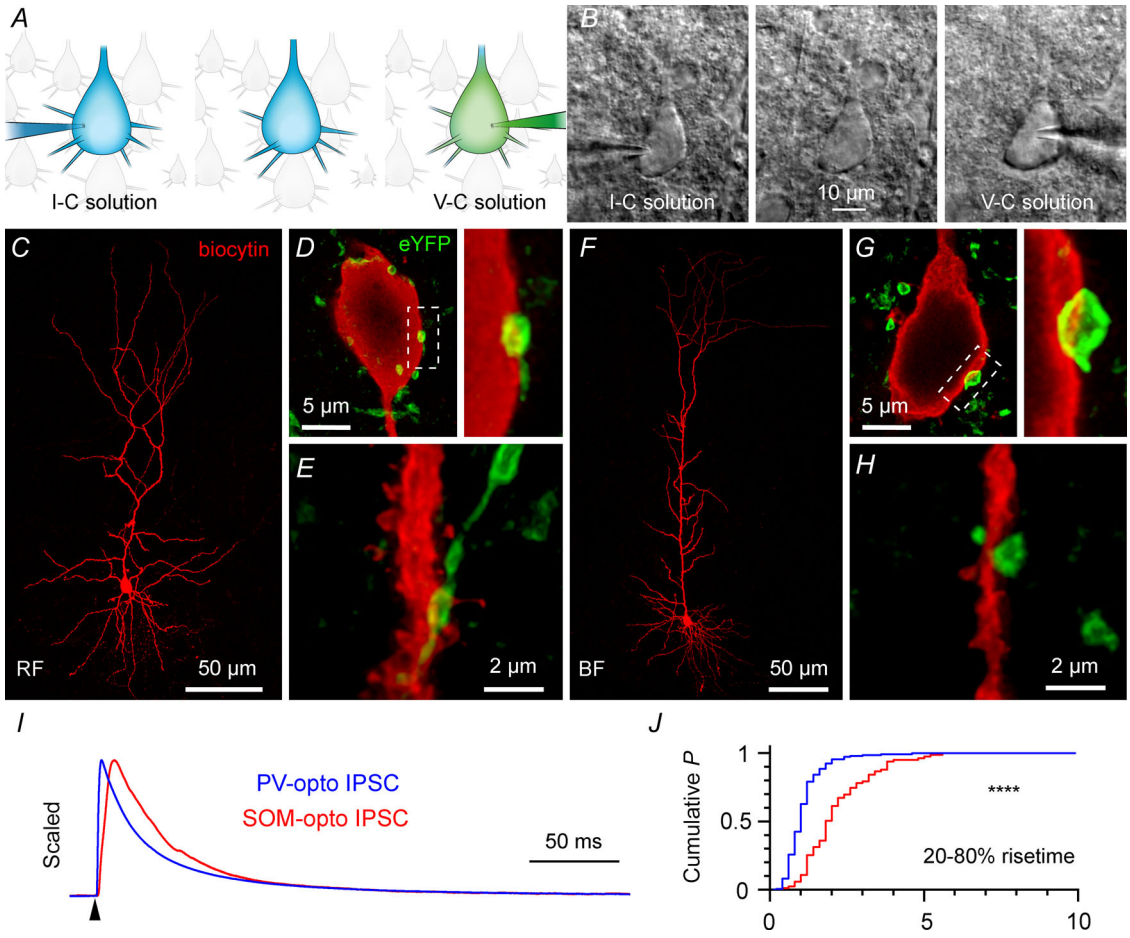

Figure 2. Sequential re-patching of the same target cell using pipettes filled with different intracellular solutions in PV-ChR2 (H134R)-eYFP and SOM-ChR2 (H134R)-eYFP mice
A, cartoon illustrating the protocol based on the use of different pipettes either filled with solution for current-clamp (I-C, blue) and voltage-clamp recordings (V-C, green). *B*, oblique illumination images of the same cell during the same steps illustrated in *A*. Note that the cell maintains a healthy morphology throughout the procedure. *C*, confocal image of a biocytin-filled regular-firing cell (RF). *D*, micrograph of putative somatic synaptic contacts identified by eYFP expression on a recorded RF pyramidal neuron from a PV-ChR2 (H134R)-eYFP mouse. The area delimited by the white dotted lines is shown at higher magnification in the inset to the right. *E*, putative dendritic synaptic contact established on an RF cell in a slice from a SOM-ChR2 (H134R)-eYFP animal. *F*, *G* and *H*, similar to *D*, *E* and *F*, respectively, but for burst-firing (BF) pyramidal cells. *I*, faster risetimes in PV- *vs.* SOM-opto IPSCs: averaged normalized traces (blue, PV-opto IPSC; red, SOM-opto IPSC). *J*, summary plot showing a clear difference in the distributions. ****$P < 0.0001$. [Colour figure can be viewed at wileyonlinelibrary.com]

result was found when comparing SOM-opto IPSCs (Fig. 3*C*, *D*). The amplitude of PV-opto IPSCs ($n = 42$ mice) recorded in $n = 80$ BFs was 2.4 nA (mean), 1.2 nA (SD) compared to 2.0 nA (mean), 1.6 nA (SD) for RFs ($n = 79$, $P < 0.001$, KS). The peak of SOM-opto IPSCs ($n = 23$ mice) recorded from RFs ($n = 38$) was 1.7 nA (mean), 1.0 nA (SD) compared to 1.3 nA (mean), 0.8 nA (SD) in BFs ($n = 45$, $P = 0.0399$ KS). Importantly, no significant differences in the series resistance associated with recordings from RFs *vs.* BFs were observed either in PV- or SOM-opto IPSC experiments. In PV-opto IPSC experiments the series resistance measured in RFs was 11.7 MΩ (mean), 4.3 MΩ (SD) compared to 12.1 MΩ (mean), 4 MΩ (SD) in BFs ($P = 0.143$, KS). Similarly, for SOM-opto IPSC experiments, the series resistance calculated for RFs was 9.3 MΩ (mean), 3.3 MΩ (SD) compared to 9.3 MΩ (mean), 3.3 MΩ (SD) in BFs ($P = 0.898$, KS).

Lastly, as shown in Fig. 4*A*, the amplitudes of PV-opto IPSCs found in RFs and BFs did not depend on the sex of the animal [RF cells: 1.9 nA (mean), 1.5 (SD) and 2.0 nA (mean), 1.8 (SD), $n = 40$ and $n = 39$ cells from male and female animals, respectively, $P = 0.855$, KS; BF cells: 2.4 nA (mean), 1.2 (SD) and 2.4 nA (mean), 1.2 (SD), $n = 48$ and 32 cells from male and female mice, $P = 0.873$, KS]. In addition, PV-opto IPSCs on RFs and BFs were recorded in animals of similar age [RF, P30 (mean), 4 days (SD) *vs.* BF, P30 (mean), 4 days (SD), MW, $P = 0.206$]. Similar conclusions were drawn when comparing SOM-opto IPSCs (Fig. 4*B*) from RFs and BFs recorded from slices prepared from animals of different sex [RFs: 2.0 nA (mean), 1.0 (SD) and 1.4 nA (mean), 0.9 (SD), $n = 19$ and $n = 19$ cells from male and female animals, respectively, $P = 0.152$, KS; BFs: 1.2 nA (mean), 0.9 (SD) and 1.3 nA (mean), 0.6 (SD), $n = 19$ and 26 cells from male and female mice, $P = 0.059$, KS] and postnatal

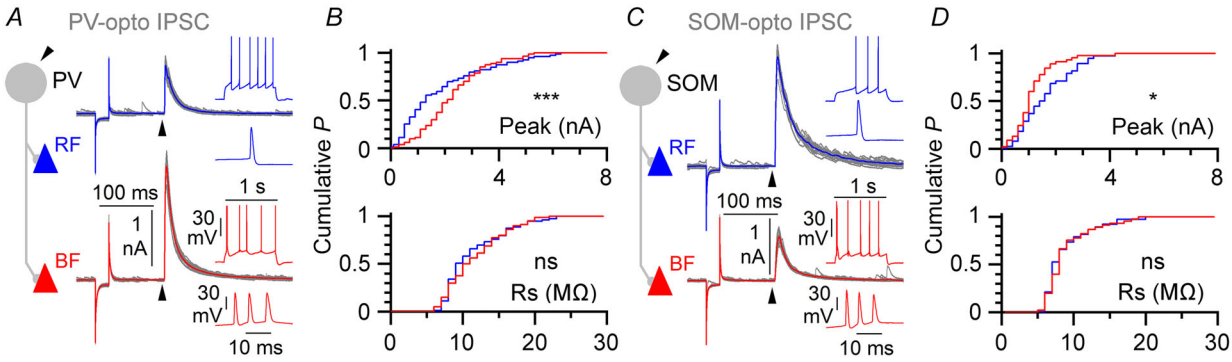

Figure 3. Pre- and postsynaptic cell type specificity of GABAergic input received by subicular PCs
A, comparison of optogenetically evoked IPSCs from PVs (PV-opto IPSCs, recorded in voltage-clamp at +10 mV) in regular-firing (RF, blue) *vs.* burst-firing (BF, red) subicular pyramidal cells. Several traces obtained at 0.1 Hz (grey, $n = 18$) are superimposed and their average is shown in blue or red for the different cell types. Firing patterns are shown in the insets, with the first action potential(s) at a magnified scale. The experimental protocol detailed in Fig. 3 was used. Series resistances (Rs) were monitored by a −10 mV step delivered before the light flash (0.5 ms, black arrowhead). *B*, summary plots. Note the different IPSC peak amplitudes (peak, top) with similar series resistances (Rs, bottom). *C* and *D*, as in *A* and *B*, but for the IPSC evoked from SOMs (SOM-opto IPSC). Note the opposite selectivity of SOMs for PC subtypes compared to PVs. $^{*}P < 0.05$, $^{***}P < 0.001$, $^{ns}P > 0.05$. [Colour figure can be viewed at wileyonlinelibrary.com]

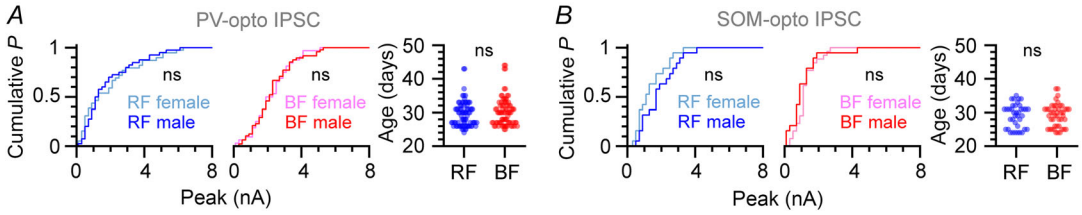

Figure 4. Neither sex nor developmental stage are variables involved in the cell type specificity of PV- and SOM opto IPSCs, under our experimental conditions
A, left: summary plots of PV-opto IPSC amplitudes recorded in regular-firing (RF) or burst-firing (BF) pyramidal cells according to the sex of the animal (female and male). Note the lack of differences between the different groups. Right: postnatal age of the mice used for individual cell recordings plotted according to the firing pattern of the neuron. *B*, same analysis as in *A*, but for SOM-opto IPSCs. No sex-related differences were found in either PV- or SOM-opto IPSCs from either RFs or BFs. Also note that RF and BF functional phenotypes were observed in slices prepared from mice without significant age difference. $^{ns}P > 0.05$. [Colour figure can be viewed at wileyonlinelibrary.com]

age [RFs, P29 (mean), 4 days (SD) *vs*. BFs, P29 (mean), 3 days (SD), MW, $P = 0.958$].

Taken together, these results suggest that the relative strength of the GABAergic IPSC provided by different types of INTs depends on the functional subtype of target PCs in a presynaptic INT-specific fashion. Perisomatic targeting PVs produce stronger IPSCs on BFs, whereas dendritic targeting SOMs generate larger events on RFs.

As neurotransmitter release is critically dependent on different types of voltage-gated calcium channels (VGCCs) expressed in presynaptic terminals (Dolphin & Lee, 2020), we compared the sensitivity of opto IPSCs to toxins selective for the main VGCCs of the CNS, i.e. N- (ω-conotoxin GVIA, cono) and P/Q-subtypes (ω-agatoxin IVA, aga) VGCCs. Our purpose was to test the hypothesis that release of GABA from either different INTs or onto functionally distinct PCs was associated with distinct proportions of cono- and aga-sensitive VGCCs.

PV-opto IPSCs recorded from RFs and BFs ($n = 29$ mice) were more sensitive to the exposure to aga than to a control solution (no toxin) or to cono. In RFs (Fig. 5*A*), evoked events were only slightly reduced by cono [72.2% (mean), 17.7% (SD) of baseline, $n = 11$ cells], but their decrease was not significantly different from the experimental drift observed in slices maintained in control solution [98.3% (mean), 16.6% (SD), $n = 14$ cells, $P = 0.127$, KWD]. In contrast, aga powerfully decreased the opto IPSC, with an effect significantly stronger than both control and cono-containing solutions [8.4% (mean), 10.1% (SD) of baseline, $n = 13$ cells, $P < 0.001$ compared to control and $P = 0.0067$ compared to cono, KWD].

The same pharmacological manipulations yielded similar results in PV-opto IPSCs of BFs (Fig. 5*B*). The reduction of the peak PV-opto IPSC in control [94.2% (mean), 12.9% (SD) of baseline, $n = 15$ cells] was not significantly different from that observed following exposure to a cono-containing solution [80.6% (mean), 13.0 (SD) of baseline, $n = 13$ cells, $P = 0.167$, KWD], whereas aga application strongly suppressed the opto IPSC [5.4% (mean), 4.6% (SD) of baseline, $n = 13$ cells, $P = 0.0022$ and $P < 0.001$ when compared to the effects of control and cono, respectively, KWD]. Importantly, there were no differences in the time-dependent change in the series resistance during recordings obtained from RFs *vs*. BFs ($P = 0.977$, $n = 31$ recordings for opto IPSCs in RF cells, and $P = 0.7868$, $n = 41$ recordings for opto IPSCs in RFs, KW).

Similar results were obtained in SOM-opto IPSCs (Fig. 6*A*, *B*, $n = 22$ mice), namely a powerful block of the evoked response by aga, compared to the non-significant effect of cono *vs*. control. Addition of aga to the external solution decreased the opto IPSC amplitude recorded from RFs to 10.4% (mean), 7.0% (SD) of the initial baseline ($n = 12$ cells), which was a stronger decline compared to that observed by maintaining slices in control solution [89.6% (mean), 9.2% (SD) of baseline, $n = 9$ cells, $P < 0.001$, KWD] or following exposure to cono [80.3% (mean), 18.7% (SD) of baseline, $n = 9$, $P = 0.0021$, KWD]. As reported above for PV-opto IPSCs, no differences were found between maintaining toxin-free control solution and cono application ($P > 0.999$, KWD). The same outcomes were observed in opto IPSCs from BFs. The amplitude of the evoked events in the presence of control solution [89.1% (mean), 10.1% (SD) of baseline, $n = 6$ cells] was not different from what was measured after the application of cono [66.6% (mean), 14.0% (SD) of baseline, $n = 11$ cells, $P = 0.285$, KWD]. In contrast, exposure to aga reduced the opto IPSC to 18.1% (mean), 8.3% (SD) of baseline ($n = 12$ cells), which was a larger effect compared to maintaining control solution ($P < 0.001$, KWD) or cono application ($P = 0.0023$, KWD). Series resistance dynamics between the various manipulations were also similar, as shown for PV-opto IPSC recordings ($P = 0.344$, $n = 30$ recordings for opto IPSCs in RFs, and $P = 0.620$, $n = 29$ recordings for opto IPSCs in BFs, KW).

Taken together, these experiments indicate that opto IPSCs generated by PVs and SOMs onto RFs and BFs depend predominantly on the activation of presynaptic aga-sensitive VGCCs, whereas the contribution of cono-sensitive VGCCs was potentially minor and did not reach statistical significance.

In addition to VGCCs, presynaptic receptors may produce a strong modulatory impact on neurotransmitter release. As mentioned in the Introduction, activation of the MOR is capable of opposing GABA release from INTs of several brain regions, including the hippocampus proper. Here, the expression of MORs has been consistently detected in PVs (Drake & Milner, 2002) where they exert powerful effects (He et al., 2021; Shao et al., 2020). In contrast, the expression and functional impact of MORs in SOMs are less clear. Therefore, we decided to assess the sensitivity of PV- and SOM-opto IPSCs to the MOR agonist DAMGO in both RFs and BFs.

As a control experiment, we initially recorded from PVs ($n = 4$ mice, Fig. 7*A*) and SOMs ($n = 2$ mice, Fig. 7*B*) under non-invasive (cell-attached and loose cell-attached) configurations to monitor the number of action potentials elicited by a single flash under our experimental conditions and to ensure the lack of major effects of DAMGO application onto the optogenetic stimulation itself. In control solution, optogenetic stimulation produced similar results in PVs and SOMs, i.e. 1.3 spikes per flash (mean), 0.4 spikes per flash (SD, $n = 9$ cells) in PVs compared to 1.3 spikes per flash (mean), 0.5 spikes per flash (SD, $n = 7$ cells) in SOMs ($P > 0.999$, MW). The addition of DAMGO did not significantly change the number of spikes per flash either in PVs or SOMs [for PVs 1.2 spikes per flash (mean), 0.4 spikes per flash (SD) in the presence of DAMGO, $P = 0.5$, W, and for SOMs 1.6 spikes per flash (mean),

0.8 spikes per flash (SD) in the presence of DAMGO, $P = 0.5$, W].

Next, we investigated the effect of DAMGO in opto IPSCs. Figure 8*A* and *B* (n = 22 mice) show the modulation of the PV-opto IPSC in RFs and BFs by DAMGO in the absence and in the presence of the broad-spectrum opioid receptor antagonist naloxone (10 μM). A significant difference in the degree of reduction of the opto IPSC was observed when DAMGO was added to control *vs.* naloxone-including solution, independently of the identity of the PC (RF or BF). In control solution, the addition of DAMGO decreased the PV-opto IPSCs of RFs to 51.9% (mean), 21.3% (SD) of baseline (n = 19 cells), whereas in the constant presence of naloxone the effect was reduced to 75.4% (mean), 19.9 (SD) of baseline ($n = 12$ cells, $P = 0.0074$, MW). Similarly, in BFs, DAMGO applied to control solutions decreased the amplitude of the opto IPSC to 62.7% (mean), 11.1% (SD) of baseline (n = 17 cells) compared to 86.6% (mean), 13.2% (SD) of baseline in the constant presence of the naloxone

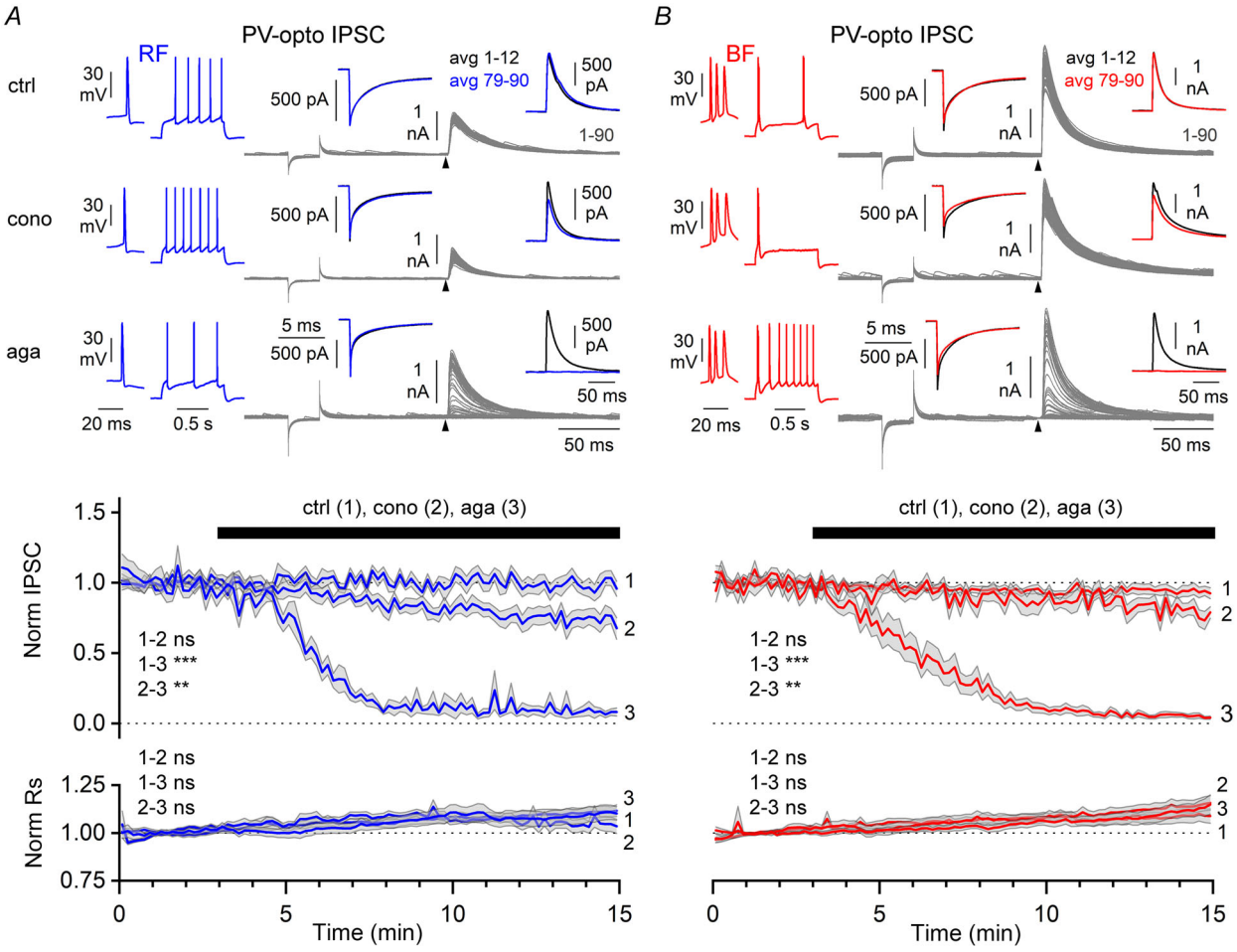

Figure 5. ω-Conotoxin GVIA (cono) and ω-agatoxin IVA (aga) added to control solution (ctrl) have similar effects on the optogenetically evoked IPSC from parvalbumin-expressing interneurons (PV-opto IPSC) in regular- (RF) and burst-firing (BF) pyramidal cells

A, recordings from RFs according to the protocol of Fig. 3. Top panels show experimental traces. Left: firing pattern in blue with an inset illustrating the first action potential of the train. Right: PV-opto IPSCs exposed to ctrl, cono or aga. Black arrowhead indicates the light flash. All sweeps of the experiment (90 traces, 1 sweep every 10 s) are in grey. Two insets show averages of the capacitive current during the −10 mV jump (left) and of the evoked IPSC (right), during the first and last 2 min of the recording [12 sweeps, average (avg) 1–12, black; avg 79–90, blue, respectively, light flash is not indicated for clarity]. Bottom panels: summary time courses of the normalized PV-opto IPSC (norm IPSC) and series resistance (norm Rs) during the different manipulations (indicated by the black bar). Ctrl, 1; cono, 2; and aga, 3. Note the major suppression of the response during aga application and the minor drifts in ctrl or cono-containing solutions. Also, note the comparable drift of the series resistance independently of the experimental manipulation. *B*, identical to *A*, but for recordings on BFs. Results are very similar to those observed in *A*. $^{**}P < 0.01$, $^{***}P < 0.001$, $^{ns}P > 0.05$. Data shown as mean ± SEM. [Colour figure can be viewed at wileyonlinelibrary.com]

($n = 9$ cells, $P < 001$, MW). Changes in series resistance dynamics could not account for the observed results, as similar drifts were observed when testing the effect of DAMGO in the absence *vs.* presence of naloxone (RFs, $P = 0.675$, MW and BFs, $P = 0.874$, MW). Although DAMGO induced a reduction of the opto IPSC amplitude in both RFs and BFs, we also noted an apparent difference in the time course of the effect, which appeared to be faster on the opto IPSC recorded from RFs, thus suggesting the presence of postsynaptic cell-dependent differences.

To understand whether this apparent effect was specific to PV-opto IPSCs, we performed identical experiments on evoked responses generated by the stimulation of SOMs. As shown in Fig. 9*A* and *B* ($n = 12$ mice), exposure of cells to DAMGO reduced the amplitude of the SOM-opto IPSCs in both RFs and BFs. In RFs, SOM-opto IPSCs were decreased by DAMGO application to 39.2% (mean), 13.7% (SD) of baseline ($n = 8$ cells) in contrast to 81.2% (mean), 10.5% (SD) of baseline when DAMGO was introduced in the constant presence of naloxone

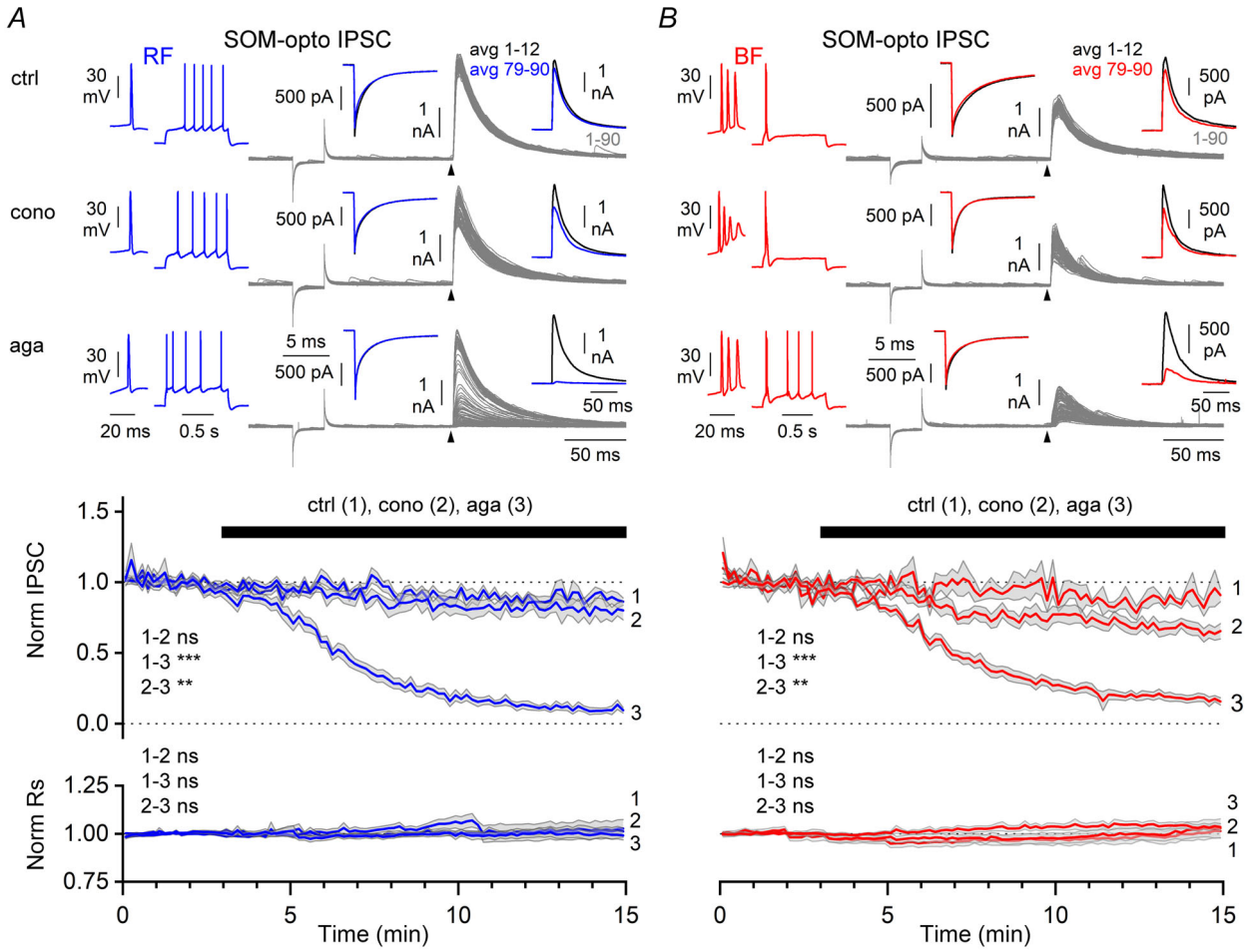

Figure 6. Similar effects of ω-conotoxin GVIA (cono) and ω-agatoxin IVA (aga) addition to control solution (ctrl) on the IPSCs optogenetically evoked from somatostatin-expressing interneurons (SOM-opto IPSC) in regular- (RF) *vs.* burst-firing (BF) pyramidal cells
A, recordings from RFs according to the protocol of Fig. 3. Top panels show experimental traces. Left: firing pattern in blue with an inset illustrating the first action potential of the train. Right: PV-opto IPSCs exposed to ctrl, cono or aga. Black arrowhead indicates the light flash. All sweeps of the experiment (90 traces, 1 sweep every 10 s) are in grey. Two insets show averages of the capacitive current during the −10 mV jump (left) and of the evoked IPSC (right), during the first and last 2 min of the recording (12 sweeps, avg 1–12, black; avg 79–90, blue, respectively, light flash is not indicated for clarity). Bottom panels: summary time courses of the normalized SOM-opto IPSC (norm IPSC) and series resistance (norm Rs) during the different manipulations (indicated by the black bar). Ctrl, 1; cono, 2; and aga, 3. Note the major suppression of the response during aga application and the minor drifts in ctrl or cono-containing solutions. Also, note the comparable drift of the series resistance independently of the experimental manipulation. *B*, identical to *A*, but for recordings on BFs. Results are very similar to those observed in *A*. $^{**}P < 0.01$, $^{***}P < 0.001$, $^{ns}P > 0.05$. Data shown as mean ± SEM. [Colour figure can be viewed at wileyonlinelibrary.com]

($P < 0.001$, MW). In the case of BFs, SOM-opto IPSCs were reduced to 42.7% (mean), 20.7% (SD) of baseline by DAMGO application ($n = 10$ cells), compared to 81.1% (mean),14.6 (SD) of baseline ($n = 9$) when DAMGO was in the additional presence of naloxone ($P < 0.001$, MW). In both sets of experiments differences could not be explained by series resistance dynamics in the absence *vs*. in the presence of naloxone (RFs, $P = 0.173$, MW and BFs, $P = 0.054$, MW).

Although the most parsimonious explanation for these results is that binding of DAMGO to presynaptic MORs decreases GABA release from PVs and SOMs, MORs are also present on glial cells. Their activation on astrocytes triggers glutamate release, which could, in principle, activate metabotropic glutamate receptors (mGluRs) on GABAergic terminals. If this were the case, the differential expression of mGluRs on boutons reaching RFs *vs*. BFs could explain the observed difference in the kinetics of DAMGO-induced suppression of the PV-opto IPSCs. We explored this possibility by applying DAMGO in the constant presence of the group I/II mGluR antagonist (*RS*)-α-methyl-4-carboxyphenylglycine (MCPG), as these are the subtypes expressed by PVs on terminals established on PCs (Kogo et al., 2004). As shown in Fig. 10*A* and *B*, application of DAMGO reduced PV-opto IPSCs in both RFs and BFs ($n = 7$ mice). In RFs the amplitude of the evoked response was decreased from 2.2 nA (mean), 1.6 nA (SD) to 1.1 nA (mean), 1.1 nA (SD) of baseline ($P = 0.001$, W, $n = 11$ cells). In BFs, the response was reduced from 2.7 nA (mean), 1.0 nA (SD) to 1.7 nA (mean), 0.7 (SD) ($P = 0.0001$, W, $n = 14$ cells). Series resistances did not change significantly at the end of the experiments (RFs, $P = 0.0537$ and BFs, $P = 0.153$, W). Thus, the pharmacological blockade of mGluRs did not modify the outcome of the experiment, which remained similar to that observed in Fig. 8.

Quantitative analysis of the kinetics of DAMGO effects (Fig. 11*A*–*C*) confirmed our impression of significant differences between RFs and BFs for PV-opto IPSCs (independently of the presence of MCPG: without MCPG, same data as Fig. 8, $P = 0.00395$, TWAR; MCPG, same data as Fig. 10, $P = 0.00367$, TWAR), whereas no difference was found for SOM-opto IPSCs (same data as Fig. 9, $P = 0.385$, TWAR).

Discussion

This work elucidates and highlights the complex interactions between different layers of neuronal diversity in subicular microcircuits. First, we show that interneurons can discriminate between postsynaptic, functionally distinct PCs by providing GABAergic IPSCs of different amplitudes to RFs *vs*. BFs. Second, we show that this type of preference is not consistent, as PVs and SOMs show opposite biases and provide larger IPSCs to different subpopulations of PCs. Lastly, despite a similar dependence of GABAergic output from PVs and SOMs onto RFs and BFs on the same classes of VGCCs, we show that the MOR-mediated modulation of GABAergic synaptic input onto RFs and BFs may vary between functionally distinct PCs depending on the class of presynaptic interneuron that gives rise to the IPSC. These data unravel a previously unknown level of organization of subicular GABAergic microcircuits driven both by pre- and postsynaptic cell type specificity.

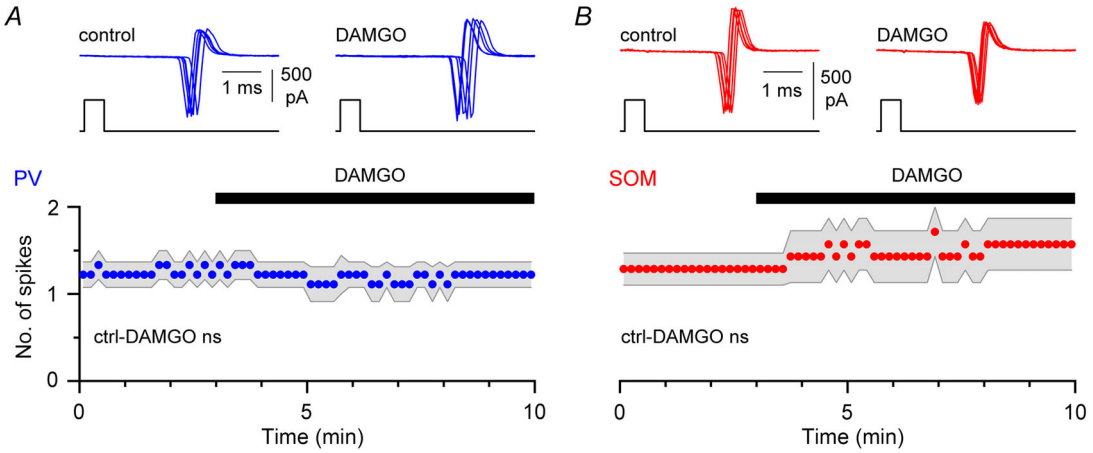

Figure 7. [D-Ala2, *N*-MePhe4, Gly-ol]-enkephalin (DAMGO) does not reduce the number of spikes in parvalbumin- (PV) or somatostatin- (SOM) expressing interneurons
A, lack of major effect of DAMGO application on the number of spikes elicited in PVs by a 0.5 ms flash. *B*, similar results in SOMs. Note that in control solution (before DAMGO application) optogenetic stimulation produces a similar number of spikes in PVs and SOMs. $^{ns}P > 0.05$. Data shown as mean ± SEM. [Colour figure can be viewed at wileyonlinelibrary.com]

The organization of subicular inhibitory microcircuits is complex and depends on different layers of neuronal diversity

It is now largely recognized that neuronal diversity of both GABAergic interneurons (Pelkey et al., 2017) and PCs (Cembrowski & Spruston, 2019) plays a critical role in determining the functions of cortical circuits, including the subicular complex (Böhm et al., 2015; Cembrowski et al., 2018; Pannuccio et al., 2012; Peng et al., 2021). Heterogeneity within specific classes of neurons at both the morphological and the physiological levels provides a critical division of labour between various cell types (Varga et al., 2012) that results in flexibility and enhanced computational power of neuronal networks (Gast et al., 2024).

Here, we have studied the diversity of subicular microcircuits by comparing opto IPSCs provided by PVs (Hu et al., 2014) and SOMs (Wu et al., 2023), which typically establish synaptic contacts with different postsynaptic domains of target cells (perisomatic *vs*. dendritic) of both RFs and BFs.

Clarifying the pre- and/or postsynaptic factors governing GABAergic IPSCs in subicular circuits is

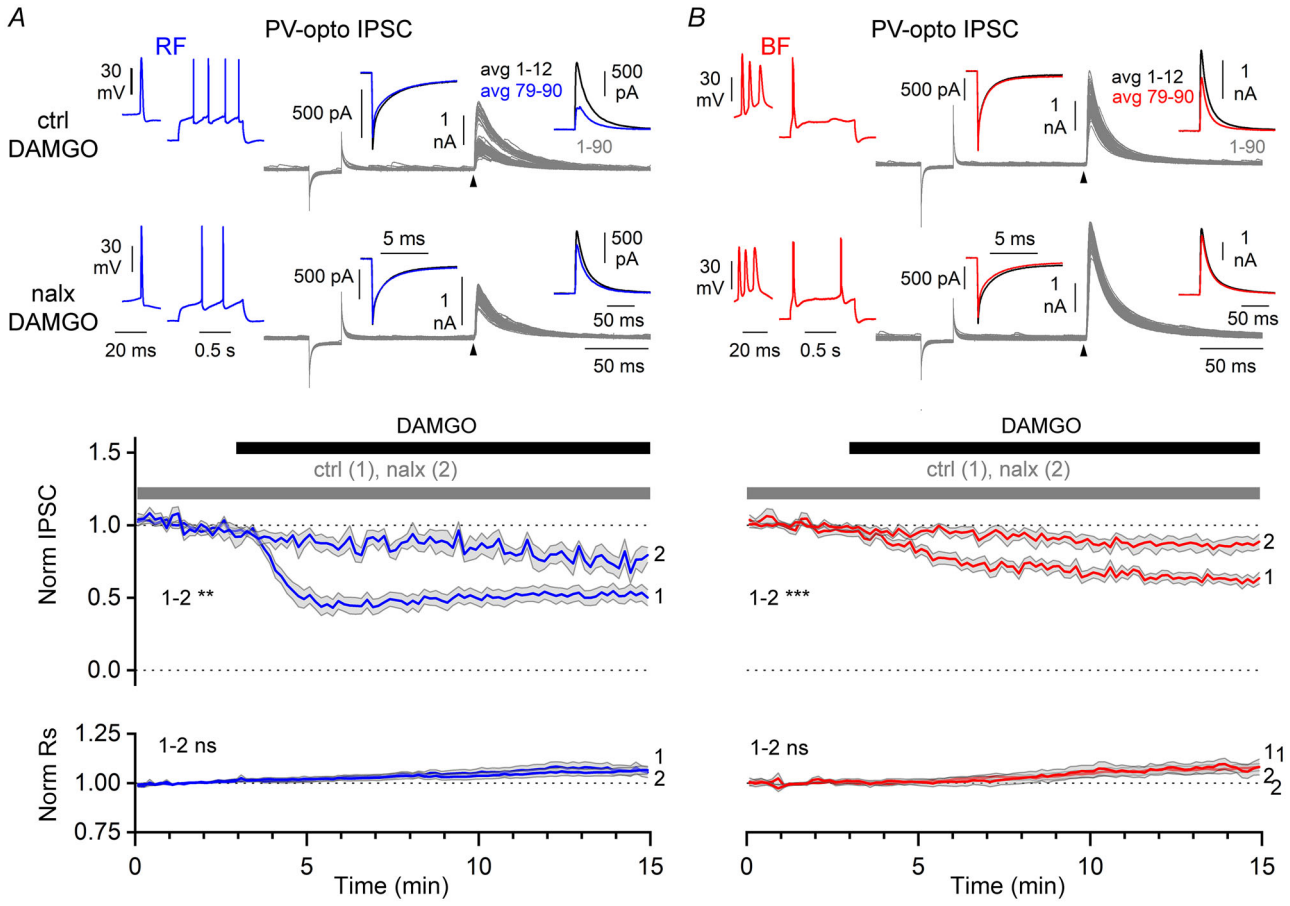

Figure 8. Effect of [D-Ala2, *N*-MePhe4, Gly-ol]-enkephalin (DAMGO) on the optogenetically evoked IPSC triggered by the stimulation of parvalbumin-expressing interneurons (PV-opto IPSC) on regular- (RF) and burst-firing (BF) pyramidal cells
A, experimental traces for RFs. Left: firing pattern is shown in blue with an inset illustrating the first action potential(s) of the train. Right: PV-opto IPSCs for RFs exposed to DAMGO in control solution (ctrl DAMGO) or in the constant presence of the opioid receptor antagonist naloxone (nalx DAMGO). Black arrowheads indicate the timing of the light flash. All sweeps of the experiment (90 traces, 1 sweep every 10 s) are shown in grey. Two insets show in detail the averages of the capacitive current during the −10 mV jump (left) and of the evoked IPSC (right), during the first and last 2 min of the recording (sweeps 1–2, avg 1–12, black; and sweeps 79–90, avg 79–90, blue, respectively, light flash is not indicated for clarity). Bottom panels: summary plots of the time courses of the normalized PV-opto IPSC (norm IPSC) and series resistance (norm Rs) during the different manipulations indicated by the black and grey bars. Control solution, ctrl (1), naloxone, nalx (2). $^{**}P < 0.01$, $^{***}P < 0.001$, $^{ns}P > 0.05$. Note the comparable drift of the series resistance independently of the experimental manipulation. *B*, identical to *A*, but for recordings on BFs. Note the slower kinetics of the DAMGO-dependent suppression of IPSCs in BFs compared to RFs. Data shown as mean ± SEM. [Colour figure can be viewed at wileyonlinelibrary.com]

also important in the light of previous studies showing the existence of parallel processing in this region, which depends on the activity of distinct types of pyramidal neurons with different gene expression, long-range and local connectivity, and electrophysiological properties (Cembrowski et al., 2018). Because of our electrophysiological approach, we have taken advantage of the classical functional distinction of subicular PCs into RFs and BFs. We show that the classification scheme is robust and does not depend, under our experimental conditions, on variables such as sex and developmental stage of the animals used. In fact, we reproduced data we had previously reported under similar experimental conditions in wild-type mice, i.e. a roughly equivalent proportion of RFs and BFs in subicular slices *ex vivo* (Fiske et al., 2020).

Our first result, i.e. that PVs produce larger opto IPSCs in BFs compared to RFs, taken together with the original reports by Lee et al. (2014) that PVs discriminate between differently anatomically located PCs in the hippocampus proper, reinforces the general idea that this class of interneuron does not form uniform/random connections with postsynaptic cells. It would be interesting to see whether

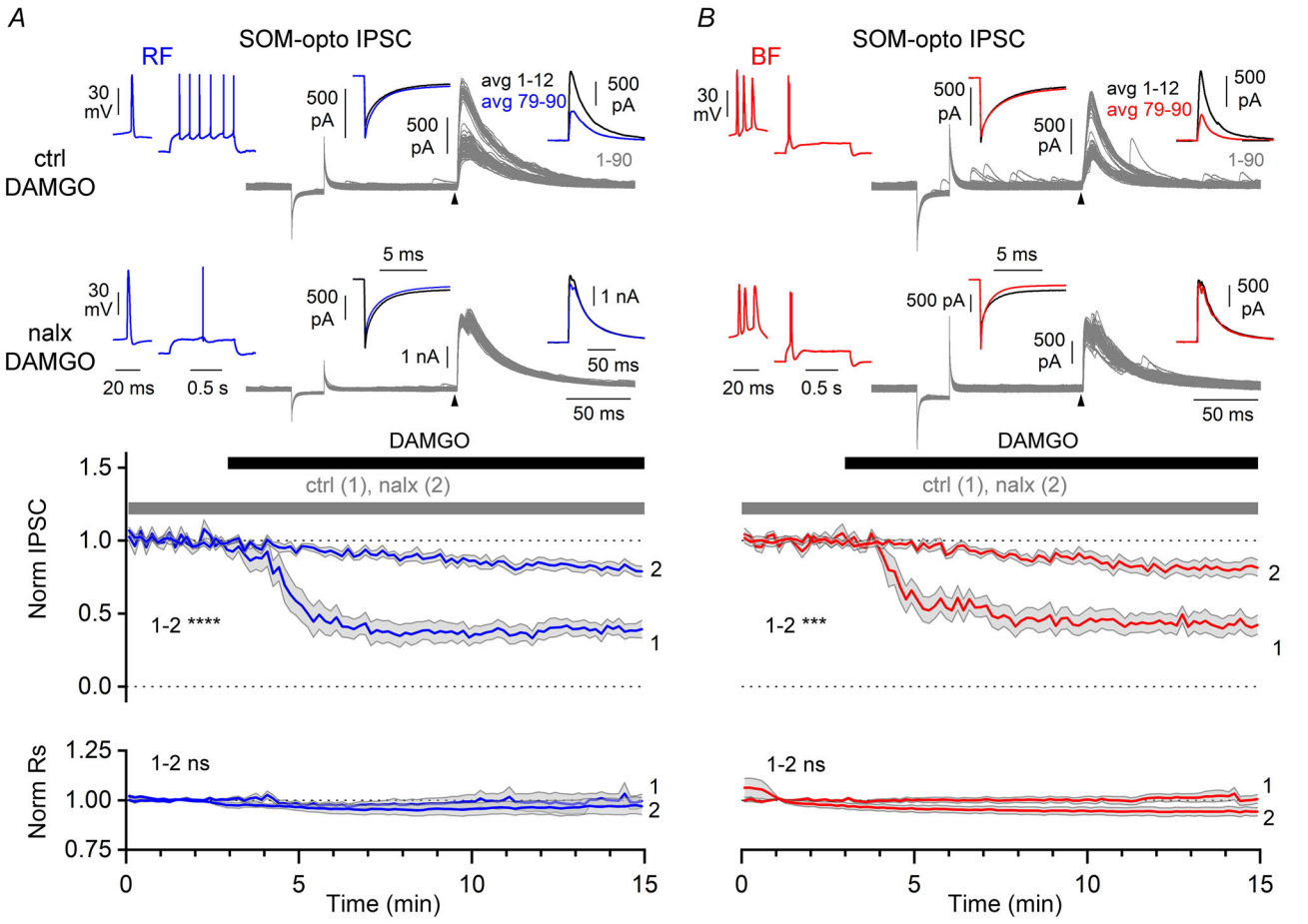

Figure 9. Effect of [D-Ala2, *N*-MePhe4, Gly-ol]-enkephalin (DAMGO) on the optogenetically evoked IPSC triggered by the stimulation of somatostatin-expressing interneurons (SOM-opto IPSC) on regular- (RF) and burst-firing (BF) pyramidal cells
A, experimental traces for RFs. Left: firing pattern is shown in blue with an inset illustrating the first action potential(s) of the train. Right: PV-opto IPSCs for RFs exposed to DAMGO in control solution (ctrl DAMGO) or in the constant presence of the opioid receptor antagonist naloxone (nalx DAMGO). Black arrowheads indicate the timing of the light flash. All sweeps of the experiment (90 traces, 1 sweep every 10 s) are shown in grey. Two insets show in detail the averages of the capacitive current during the −10 mV jump (left) and of the evoked IPSC (right), during the first and last 2 min of the recording (sweeps 1–2, avg 1–12, black; and sweeps 79–90, avg 79–90, blue, respectively, light flash is not indicated for clarity). Bottom panels: summary plots of the time courses of the normalized PV-opto IPSC (norm IPSC) and series resistance (norm Rs) during the different manipulations indicated by the black and grey bars. Control solution, ctrl (1), naloxone, nalx (2). $^{***}P < 0.001$, $^{****}P < 0.0001$, $^{ns}P > 0.05$. Note the comparable drift of the series resistance independently of the experimental manipulation. *B*, identical to *A*, but for recordings on BFs. Note the similar kinetics of the DAMGO-dependent suppression of IPSCs in BFs and RFs. Data shown as mean ± SEM. [Colour figure can be viewed at wileyonlinelibrary.com]

the anatomically distinguished pyramidal neurons of the study of Lee et al. (2014) are also endowed with different excitability, which could suggest an even more general organizing principle based on function.

At present, apart from this study, no data comparing the cell type specific GABAergic input received by functionally distinct subicular pyramidal neurons are available. Assuming that GABA released by PVs contributes to the activation of extrasynaptic GABAa receptors, our results would appear consistent with the observation of Pannuccio et al. (2012), that somatically recorded tonic GABAergic currents are larger in subicular BFs compared to RFs. In contrast, our results would seem opposite to what was reported by Böhm et al. (2015), as they showed larger compound IPSCs in RFs compared to BFs during spontaneously occurring sharp-wave-associated ripples in slices. However, it is difficult to rigorously evaluate the consistency/inconsistency of our data with these aforementioned studies because we have quantified strictly PV- and SOM-originated inputs under static conditions, whereas both the tonic currents and the dynamic compound IPSCs mentioned above could include contributions from other interneuron subtypes.

Importantly, we expand the notion of interneuron postsynaptic PC selectivity originally discovered by Varga et al. (2010) and Lee et al. (2014) in PVs by showing that SOMs also distinguish between postsynaptic targets, albeit with an opposite bias.

The bidirectional dependency on the presynaptic type of interneuron indicates that our measurements are unlikely to depend on systematic voltage-clamp errors favouring larger IPSCs in one postsynaptic subtype *vs.* the other. Although structural differences in the dendritic arborizations (Fiske et al., 2020, but see also Staff et al., 2000) and in the resting membrane properties

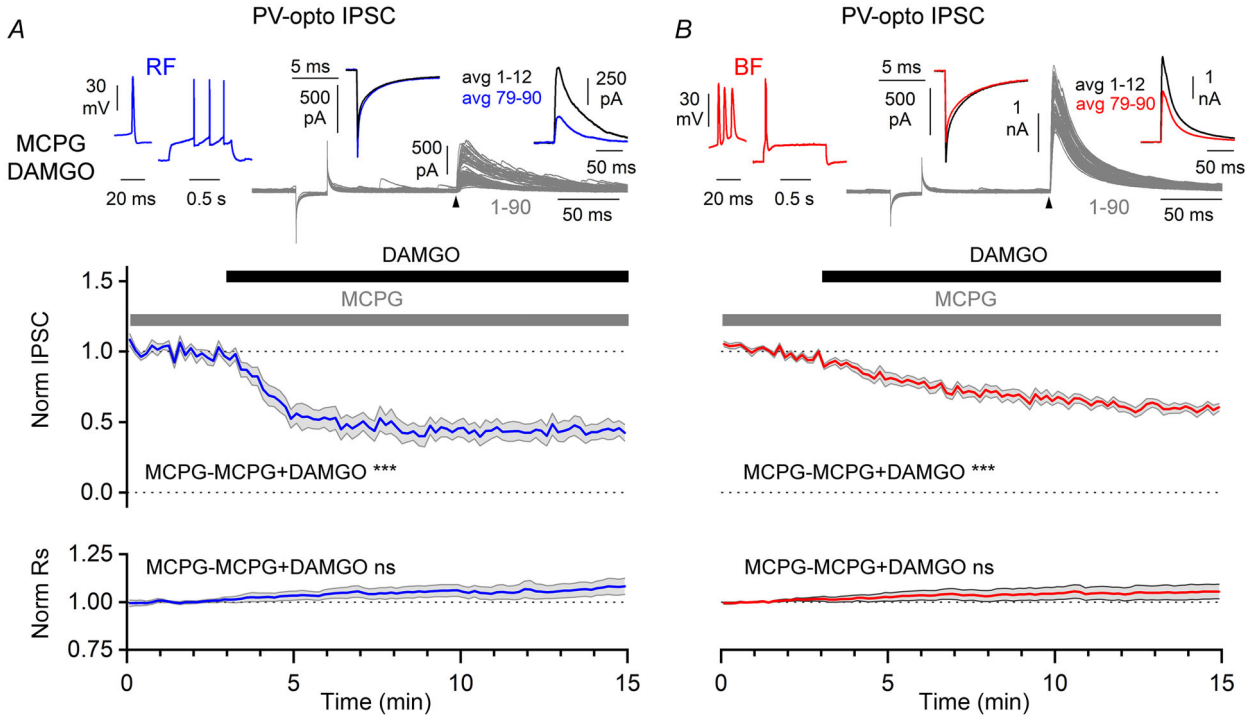

Figure 10. [D-Ala2, *N*-MePhe4, Gly-ol]-enkephalin (DAMGO) application in the constant presence of (*RS*)-α-methyl-4-carboxyphenylglycine (MCPG) suppresses the optogenetically evoked IPSC triggered by the stimulation of parvalbumin-expressing interneurons (PV-opto IPSC) both in regular- (RF) and burst-firing (BF) pyramidal cells.
A, experimental traces for RFs. Left: firing pattern is shown in blue with an inset illustrating the first action potential(s) of the train. Right: PV-opto IPSCs for RFs exposed to DAMGO in MCPG-containing solution (MCPG DAMGO). Black arrowheads indicate the timing of the light flash. All sweeps of the experiment (90 traces, 1 sweep every 10 s) are shown in grey. Two insets show in detail the averages of the capacitive current during the −10 mV jump (left) and of the evoked IPSC (right), during the first and last 2 min of the recording (sweeps 1–2, avg 1–12, black; and sweeps 79–90, avg 79–90, blue, respectively, light flash is not indicated for clarity). Bottom panels: summary plots of the time courses of the normalized PV-opto IPSC (norm IPSC) and series resistance (norm Rs) during the pharmacological manipulation indicated by the black and grey bars. $^{***}P < 0.001$, $^{ns}P > 0.05$. Note the comparable (non-significant) drift of the series resistance independently of the experimental manipulation. *B*, identical to *A*, but for recordings on BFs similarly to that illustrated in Fig. 9. Data shown as mean ± SEM. [Colour figure can be viewed at wileyonlinelibrary.com]

of RFs and BFs (Staff et al., 2000) have been reported, our experimental approach was tailored to minimize these potential problems by recording events with intracellular solutions containing blockers of non-synaptic conductances at high concentrations. We also ensured that there were no systematic differences in series resistance between recordings from RFs *vs*. BFs. Lastly, the optogenetic stimulus that was used to activate PVs and SOMs was chosen to be short to trigger in both interneuron subtypes about one spike and, as reported in the Results, no significant differences were detected in the number of spikes triggered in PVs *vs*. SOMs.

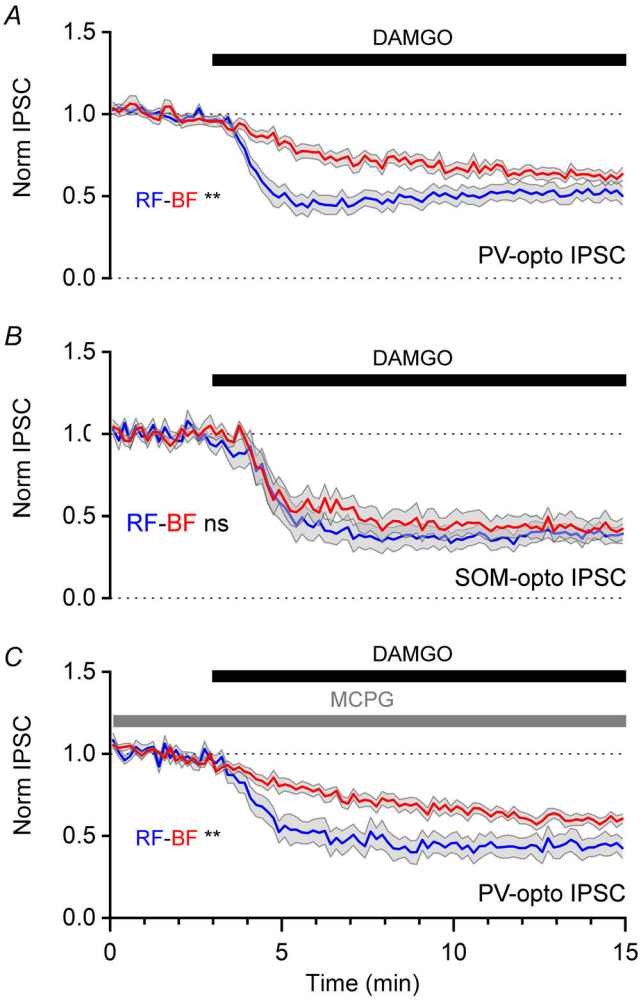

Figure 11. Pre- and postsynaptic cell type specificity regulation of the kinetics of the suppression of optogenetically evoked IPCSs by [D-Ala2, *N*-MePhe4, Gly-ol]-enkephalin (DAMGO) onto subicular pyramidal cells
A, time course of the reduction of the optogenetically evoked IPSC triggered by the stimulation of parvalbumin-expressing interneurons (PV-opto IPSC) in regular- (RF) and burst-firing (BF) cells superimposed. Note the clearly faster onset of the suppression of the PV-opto IPSC in RFs. *B*, same analysis as in *A* performed on the optogenetically evoked IPSC triggered by the stimulation of somatostatin-expressing interneurons (SOM-opto IPSC). Note the kinetic similarity in the decrease of the SOM-opto IPSC in RFs and BFs. *C*, the kinetic difference in *A* is not mediated by MCPG-sensitive mGluRs as it persists in the constant presence of the antagonist. Data from Figs 9, 10 and 11 (*A, B* and *C*, respectively). $^{**}P < 0.01$, $^{ns}P > 0.05$. Data shown as mean ± SEM. [Colour figure can be viewed at wileyonlinelibrary.com]

Interestingly, in contrast to the postsynaptic cell specificity of IPSC amplitudes, we found a rather uniform IPSC dependency on different classes of VGCCs, irrespective of the presynaptic interneuron (PV *vs*. SOM) generating the opto IPSC. In all cases, it was clear that opto IPSCs depended predominantly on aga-sensitive P/Q VGCCs. While a similar dependency of PV-generated IPSCs on aga-sensitive P/Q calcium channels has been reported in both hippocampal granule cells and PCs (Hefft & Jonas, 2005; Lee et al., 2011), to our knowledge, this type of experiment has not been performed for SOM-generated IPSCs. In agreement with the apparent lack of a major asynchronous component of the SOM-opto IPSC, we found a major dependency on aga-sensitive channels in both RFs and BFs.

Cell type specificity of μ opioid receptor regulation of subicular GABAergic networks

VGCCs are modulated in many regions by opioid receptors (Weiss & Zamponi, 2021). Therefore, given the similar sensitivity to aga and cono of the PV- and SOM-opto IPSCs, the different kinetic modulation of the PV-opto IPSCs observed in response to DAMGO between RFs and BFs is surprising.

In addition to the reasons discussed in the previous paragraph, we can exclude differences in voltage-clamp between RFs and BFs as contributing factors to the different kinetics of the DAMGO effect in RFs *vs*. BFs because this specificity was only observed for PV-opto IPSCs, but not for SOM-opto IPSCs. Also, the possibility that DAMGO downregulation of PV-opto IPSC was due to the activation of MORs on astrocytes, thereby triggering glutamate release (Woo et al., 2018) with the ensuing activation of group I/II mGluR expressed by PVs (Barnes et al., 2015; Kogo et al., 2004; Sun et al., 2009; van Hooft et al., 2000), was ruled out using the group I/II antagonist MCPG.

We propose that the most parsimonious explanation for the different kinetics of DAMGO effects in RFs *vs*. BFs is that the terminals of PVs forming synaptic contacts onto RFs express a higher density of MORs, while maintaining a similar density of their molecular targets. Although presynaptic VGCCs are a probable target (Weiss & Zamponi, 2021), more work is required to either validate or disprove this hypothesis and alternative scenarios remain entirely possible. For example, another possibility could be the existence of different biochemical pathways and DAMGO-triggered second messengers mediating the observed effects.

Lastly, it is critical to underline that the effects of MOR activation *in vivo* are probably rapid and depend on non-equilibrium conditions (Banghart et al., 2018; Ma et al., 2023). In contrast to the prolonged application of DAMGO (an enkephalin derivative that resists proteolysis) in slices, release of natural agonists at the MOR do not suffer from the same limitation of DAMGO slice superfusion, which needs a long time to diffuse to its site of action in the tissue and persists because of its resistance to proteolysis. Therefore, our experimental results are likely to underestimate the real difference in sensitivity to MOR activation of PV-opto IPSCs occurring in RFs *vs*. BFs. The use of newly developed caged DAMGO compounds (Ma et al., 2023) or other light-activated opioid drugs (McClain et al., 2023) will be able to directly address this issue. This approach has the potential to show a dramatically altered level of GABAergic inhibition in RFs *vs*. BFs, and to allow a more refined investigation of the cell type specific functions of GABAergic inhibition *in vitro* and *in vivo*.

References

Anstötz, M., Fiske, M. P., & Maccaferri, G. (2021). Impaired KCC2 function triggers interictal-like activity driven by parvalbumin-expressing interneurons in the isolated subiculum in vitro. *Cerebral Cortex*, **31**(5), 4681–4698.

Banghart, M. R., He, X. J., & Sabatini, B. L. (2018). A caged enkephalin optimized for simultaneously probing mu and delta opioid receptors. *American Chemical Society Chemical Neuroscience*, **9**(4), 684–690.

Barnes, S. A., Pinto-Duarte, A., Kappe, A., Zembrzycki, A., Metzler, A., Mukamel, E. A., Lucero, J., Wang, X., Sejnowski, T. J., Markou, A., & Behrens, M. M. (2015). Disruption of mGluR5 in parvalbumin-positive interneurons induces core features of neurodevelopmental disorders. *Molecular Psychiatry*, **20**(10), 1161–1172.

Behr, J., Empson, R. M., Schmitz, D., Gloveli, T., & Heinemann, U. (1996), Electrophysiological properties of rat subicular neurons in vitro. *Neuroscience Letters*, **220**(1), 41–44.

Benini, R., & Avoli, M. (2005). Rat subicular networks gate hippocampal output activity in an in vitro model of limbic seizures. *The Journal of Physiology*, **566**(Pt 3), 885–900.

Böhm, C., Peng, Y., Maier, N., Winterer, J., Poulet, J. F., Geiger, J. R., & Schmitz, D. (2015). Functional diversity of subicular principal cells during hippocampal ripples. *Journal of Neuroscience*, **35**(40), 13608–13618.

Böhm, C., Peng, Y., Geiger, J. R. P., & Schmitz, D. (2018). Routes to, from and within the subiculum. *Cell and Tissue Research*, **373**(3), 557–563.

Cembrowski, M. S., Phillips, M. G., DiLisio, S. F., Shields, B. C., Winnubst, J., Chandrashekar, J., Bas, E., & Spruston, N. (2018). Dissociable structural and functional hippocampal outputs via distinct subiculum cell classes. *Cell*, **173**(5), 1280–1292.

Cembrowski, M. S., & Spruston, N. (2019). Heterogeneity within classical cell types is the rule: Lessons from hippocampal pyramidal neurons. *Nature Reviews Neuroscience*, **20**(4), 193–204.

Cohen, I., Navarro, V., Clemenceau, S., Baulac, M., & Miles, R. (2002). On the origin of interictal activity in human temporal lobe epilepsy in vitro. *Science*, **298**(5597), 1418–1421.

Colbert, C. M., & Johnston, D. (1996). Axonal action-potential initiation and Na^+ channel densities in the soma and axon initial segment of subicular pyramidal neurons. *Journal of Neuroscience*, **16**(21), 6676–6686.

de Guzman, P., Inaba, Y., Biagini, G., Baldelli, E., Mollinari, C., Merlo, D., & Avoli, M. (2006). Subiculum network excitability is increased in a rodent model of temporal lobe epilepsy. *Hippocampus*, **16**(10), 843–860.

Deuchars, J., & Thomson, A. M. (1996). CA1 pyramid-pyramid connections in rat hippocampus in vitro: dual intracellular recordings with biocytin filling. *Neuroscience*, **74**(4), 1009–1018.

Dolphin, A. C., & Lee, A. (2020). Presynaptic calcium channels: specialized control of synaptic neurotransmitter release. *Nature Reviews Neuroscience*, **21**(4), 213–229.

Drake, C. T., & Milner, T. A. (2002). Mu opioid receptors are in discrete hippocampal interneuron subpopulations. *Hippocampus*, **12**(2), 119–136.

Fiske, M. P., Anstötz, M., Welty, L. J., & Maccaferri, G. (2020). The intrinsic cell type-specific excitatory connectivity of the developing mouse subiculum is sufficient to generate synchronous epileptiform activity. *The Journal of Physiology*, **598**(10), 1965–1985.

Greene, J. R., & Totterdell, S. (1997). Morphology and distribution of electrophysiologically defined classes of pyramidal and nonpyramidal neurons in rat ventral subiculum in vitro. *Journal of Comparative Neurology*, **380**(3), 395–408.

Gasparini, S., Migliore, M., & Magee, J. C. (2004). On the initiation and propagation of dendritic spikes in CA1 pyramidal neurons. *Journal of Neuroscience*, **24**(49), 11046–11056.

Gast, R., Solla, S. A., & Kennedy, A. (2024). Neural heterogeneity controls computations in spiking neural networks. *Proceedings of the National Academy of Sciences of the USA*, **121**(3), e2311885121.

Golding, N. L., & Spruston, N. (1998). Dendritic sodium spikes are variable triggers of axonal action potentials in hippocampal CA1 pyramidal neurons. *Neuron*, **21**(5), 1189–1200.

Guzman, S. J., Schlögl, A., Frotscher, M., & Jonas, P. (2016). Synaptic mechanisms of pattern completion in the hippocampal CA3 network. *Science*, **353**(6304), 1117–1123.

He, X. J., Patel, J., Weiss, C. E., Ma, X., Bloodgood, B. L., & Banghart, M. R. (2021). Convergent, functionally independent signaling by mu and delta opioid receptors in hippocampal parvalbumin interneurons. *eLife*, **10**, e69746.

Hefft, S., & Jonas, P. (2005). Asynchronous GABA release generates long-lasting inhibition at a hippocampal interneuron-principal neuron synapse. *Nature Neuroscience*, **8**(10), 1319–1328.

Hu, H., Gan, J., & Jonas, P. (2014). Interneurons. Fast-spiking, parvalbumin+ GABAergic interneurons: From cellular design to microcircuit function. *Science*, **345**(6196), 1255263.

Huberfeld, G., Wittner, L., Clemenceau, S., Baulac, M., Kaila, K., Miles, R., & Rivera, C. (2007). Perturbed chloride homeostasis and GABAergic signaling in human temporal lobe epilepsy. *Journal of Neuroscience*, **27**(37), 9866–9873.

Huberfeld, G., Menendez de la Prida, L., Pallud, J., Cohen, I., Le van Quyen, M., Adam, C., Clemenceau, S., Baulac, M., & Miles, R. (2011). Glutamatergic pre-ictal discharges emerge at the transition to seizure in human epilepsy. *Nature Neuroscience*, **14**(5), 627–634.

Jarsky, T., Mady, R., Kennedy, B., & Spruston, N. (2008). Distribution of bursting neurons in the CA1 region and the subiculum of the rat hippocampus. *Journal of Comparative Neurology*, **506**(4), 535–547.

Kim, Y., & Spruston, N. (2012). Target-specific output patterns are predicted by the distribution of regular-spiking and bursting pyramidal neurons in the subiculum. *Hippocampus*, **22**(4), 693–706.

Kogo, N., Dalezios, Y., Capogna, M., Ferraguti, F., Shigemoto, R., & Somogyi, P. (2004). Depression of GABAergic input to identified hippocampal neurons by group III metabotropic glutamate receptors in the rat. *European Journal of Neuroscience*, **19**(10), 2727–2740.

Lee, S.-H., Marchionni, I., Bezaire, M., Varga, C., Danielson, N., Lovett-Barron, M., Losonczy, A., & Soltesz, I. (2014). Parvalbumin-positive basket cells differentiate among hippocampal pyramidal cells. *Neuron*, **82**(5), 1129–1144.

Lee, S. Y., Földy, C., Szabadics, J., & Soltesz, I. (2011). Cell-type-specific CCK2 receptor signaling underlies the cholecystokinin-mediated selective excitation of hippocampal parvalbumin-positive fast-spiking basket cells. *Journal of Neuroscience*, **31**(30), 10993–11002.

Lévesque, M., & Avoli, M. (2020). The subiculum and its role in focal epileptic disorders. *Reviews in the Neurosciences*, **32**(3), 249–273.

Ma, X., Johnson, D. A., He, X. J., Layden, A. E., McClain, S. P., Yung, J. C., Rizzo, A., Bonaventura, J., & Banghart, M. R. (2023). In vivo photopharmacology with a caged mu opioid receptor agonist drives rapid changes in behavior. *Nature Methods*, **20**(5), 682–685.

MacCaferri, G., & Lacaille, J. C. (2003). Interneuron diversity series: Hippocampal interneuron classifications–making things as simple as possible, not simpler. *Trends in Neuroscience (Tins)*, **26**(10), 564–571.

McClain, S. P., Ma, X., Johnson, D. A., Johnson, C. A., Layden, A. E., Yung, J. C., Lubejko, S. T., Livrizzi, G., He, X. J., Zhou, J., Chang-Weinberg, J., Ventriglia, E., Rizzo, A., Levinstein, M., Gomez, J. L., Bonaventura, J., Michaelides, M., & Banghart, M. R. (2023). In vivo photopharmacology with light-activated opioid drugs. *Neuron*, **111**(24), 3926–3940.e10.

Marino, M., Misuri, L., & Brogioli, D. (2014). A new open source software for the calculation of the liquid junction potential between two solutions according to the stationary Nernst-Planck equation. *arXiv*. https://arxiv.org/abs/1403.3640v2

Mattia, D., Hwa, G. G., & Avoli, M. (1993). Membrane properties of rat subicular neurons in vitro. *Journal of Neurophysiology*, **70**(3), 1244–1248.

Menendez de la Prida, L. M. (2003). Control of bursting by local inhibition in the rat subiculum in vitro. *The Journal of Physiology*, **549**(Pt 1), 219–230.

Menendez de la Prida, L. M., Suarez, F., & Pozo, M. A. (2003). Electrophysiological and morphological diversity of neurons from the rat subicular complex in vitro. *Hippocampus*, **13**(6), 728–744.

Miles, R., Tóth, K., Gulyás, A. I., Hájos, N., & Freund, T. F. (1996). Differences between somatic and dendritic inhibition in the hippocampus. *Neuron*, **16**(4), 815–823.

Miles, R., Blaesse, P., Huberfeld, G., Wittner, L., & Kaila, K. (2012). Chloride homeostasis and GABA signaling in temporal lobe epilepsy. In J. L. Noebels, M. Avoli, & M. A. Rogawski, et al. (Eds.), *Jasper's Basic Mechanisms of the Epilepsies [Internet]* 4th edition. Bethesda (MD): National Center for Biotechnology Information (US).

O'Mara, S. M., Sanchez-Vives, M. V., Brotons-Mas, J. R., & O'Hare, E. (2009). Roles for the subiculum in spatial information processing, memory, motivation and the temporal control of behavior. *Progress in Neuro-Psychopharmacology & Biological Psychiatry*, **33**(5), 782–790.

Palma, E., Amici, M., Sobrero, F., Spinelli, G., di Angelantonio, S., Ragozzino, D., Mascia, A., Scoppetta, C., Esposito, V., Miledi, M., & Eusebi, F. (2006). Anomalous levels of Cl- transporters in the hippocampal subiculum from temporal lobe epilepsy patients make GABA excitatory. *Proceedings National Academy of Science USA*, **103**(22), 8465–8468.

Panuccio, G., Vicini, S., & Avoli, M. (2012). Cell type-specific properties of subicular GABAergic currents shape hippocampal output firing mode. *PLoS ONE*, **7**(12), e50241.

Pelkey, K. A., Chittajallu, R., Craig, M. T., Tricoire, L., Wester, J. C., & McBain, C. J. (2017). Hippocampal GABAergic inhibitory interneurons. *Physiological Reviews*, **97**(4), 1619–1747.

Peng, Y., Barreda Tomas, F. J., Pfeiffer, P., Drangmeister, M., Schreiber, S., Vida, I., & Geiger, J. R. P. (2021). Spatially structured inhibition defined by polarized parvalbumin interneuron axons promotes head direction tuning. *Science Advances*, **7**(25), eabg4693.

Reeves, K. C., Shah, N., Muñoz, B., & Atwood, B. K. (2022). Opioid receptor-mediated regulation of neurotransmission in the brain. *Frontiers in Molecular Neuroscience*, **15**, 919773.

Shao, C., Chen, P., Chen, Q., Zhao, M., Zhang, W. N., & Yang, K. (2020). Mu opioid receptors inhibit GABA release from parvalbumin interneuron terminals onto CA1 pyramidal cells. *Biochemical and Biophysical Research Communications*, **522**(4), 1059–1062.

Somogyi, P., & Klausberger, T. (2005). Defined types of cortical interneurone structure space and spike timing in the hippocampus. *The Journal of Physiology*, **562**(Pt 1), 9–26.

Staff, N. P., Jung, H. Y., Thiagarajan, T., Yao, M., & Spruston, N. (2000). Resting and active properties of pyramidal neurons in subiculum and CA1 of rat hippocampus. *Journal of Neurophysiology*, **84**(5), 2398–2408.

Sun, Q. Q., Zhang, Z., Jiao, Y., Zhang, C., Szabó, G., & Erdelyi, F. (2009). Differential metabotropic glutamate receptor expression and modulation in two neocortical inhibitory networks. *Journal of Neurophysiology*, **101**(5), 2679–2692.

Taube, J. S. (1993) Electrophysiological properties of neurons in the rat subiculum in vitro. *Experimental Brain Research*, **96**(2), 304–318.

van Hooft, J. A., Giuffrida, R., Blatow, M., & Monyer, H. (2000). Differential expression of group I metabotropic glutamate receptors in functionally distinct hippocampal interneurons. *Journal of Neuroscience*, **20**(10), 3544–3551.

Varga, C., Lee, S. Y., & Soltesz, I. (2010). Target-selective GABAergic control of entorhinal cortex output. *Nature Neuroscience*, **13**(7), 822–824.

Varga, C., Golshani, P., & Soltesz, I. (2012). Frequency-invariant temporal ordering of interneuronal discharges during hippocampal oscillations in awake mice. *Proceedings of the National Academy of Sciences of the USA*, **109**(4), E2726-2734.

Wang, Y., Xu, C., Xu, Z., Ji, C., Liang, J., Wang, Y., Chen, B., Wu, X., Gao, F., Wang, S., Guo, Y., Li, X., Luo, J., Duan, S., & Chen, Z. (2017). Depolarized GABAergic signaling in subicular microcircuits mediates generalized seizure in temporal lobe epilepsy. *Neuron*, **95**(1), 92–105.

Weiss, N., & Zamponi, G. W. (2021). Opioid receptor regulation of neuronal voltage-gated calcium channels. *Cellular and Molecular Neurobiology*, **41**(5), 839–847.

Woo, D. H., Bae, J. Y., Nam, M. H., An, H., Ju, Y. H., Won, J., Choi, J. H., Hwang, E. M., Han, K. S., Bae, Y. C., & Lee, C. J. (2018). Activation of astrocytic mu-opioid receptor elicits fast glutamate release through TREK-1-containing K2P channel in hippocampal astrocytes. *Frontiers in Cellular Neuroscience*, **12**, 319.

Wu, S. J., Sevier, E., Dwivedi, D., Saldi, G. A., Hairston, A., Yu, S., Abbott, L., Choi, D. H., Sherer, M., Qiu, Y., Shinde, A., Lenahan, M., Rizzo, D., Xu, Q., Barrera, I., Kumar, V., Marrero, G., Prönneke, A., Huang, S., … Fishell, G. (2023). Cortical somatostatin interneuron subtypes form cell-type-specific circuits. *Neuron*, **111**(17), 2675–2692. e9.

Additional information

Data availability statement

Data supporting the conclusions of the study are included in the paper. Raw data and analysis files will be made available to interested investigators via the Northwestern University Research and Data Repository (https://arch.library.northwestern.edu/).

Competing interests

The authors declare no competing interests.

Author contributions

G.M. designed the study. N.C.B. performed all the electrophysiological experiments. N.C.B. and G.M. analysed the data and prepared figures. M.A. analysed the confocal images and prepared figures. All authors interpreted the data. G.M. wrote the first version of the manuscript and all authors contributed important edits for intellectual content. All authors approved the final version of the paper and agree to be accountable for all aspects of the work.

Funding

This work was supported by the National Institute of Neurological Disease and Stroke (Grant NS096092 to G.M.).

Acknowledgements

The authors thank Dr Marco Martina for comments on the initial version of the manuscript and Miss Jessica Sciaky for excellent technical assistance.

Keywords

channelrhodopsin, epilepsy, interneuron, network, synaptic transmission

Supporting information

Additional supporting information can be found online in the Supporting Information section at the end of the HTML view of the article. Supporting information files available:

Peer Review History